Geomorphology 244 (2015) 56–73

Contents lists available at ScienceDirect

Geomorphology

journal homepage: www.elsevier.com/locate/geomorph

Swiftness of biomorphodynamics in Lilliput- to Giant-sized rivers and deltas

Maarten G. Kleinhans [a,*], Christian Braudrick [b], Wout M. van Dijk [d], Wietse I. van de Lageweg [c], Roy Teske [a], Mijke van Oorschot [a,e]

[a] Faculty of Geosciences, Utrecht University, PO Box 80115, 3508 TC Utrecht, The Netherlands
[b] Department of Earth and Planetary Sciences, University of California, Santa Cruz, 1156 High Street, Santa Cruz, CA 95064, USA
[c] Discipline of Geography and Spatial Sciences, School of Land and Food, University of Tasmania, Private Bag 76, Hobart, Tasmania 7001, Australia
[d] Department of Geography, Durham University, South Road, Durham DH1 3LE, UK
[e] Deltares, PO Box 177, 2600MH Delft, The Netherlands

ARTICLE INFO

Article history:
Received 4 July 2014
Received in revised form 15 April 2015
Accepted 22 April 2015
Available online 3 May 2015

Keywords:
Biogeomorphology
Experiments
Scaling
River patterns
Vegetation
Floodplain

ABSTRACT

Physical experiments of self-formed river channels and floodplains with live vegetation are pathways for understanding that complement numerical modelling. Recent experiments succeeded in creating braided rivers and dynamic meandering systems with clastic and vegetated floodplains. However, application of the insights gained from such experiments to natural systems depends on understanding potential scale effects, temporal, and spatial. Here we combine review, analysis, and experiments to identify fundamental problems of biomorphological river pattern formation that are open for further research in experiments. We first show by review and analysis that physics-based, linear bar theory predicts negligible spatial scale effects in bar and bend wavelength relative to channel width. Time scaling, on the other hand, remains problematic because it integrates multiple processes of sediment transport, floodplain formation, and bank failure affected by bank stratigraphy and riparian vegetation. As a tentative solution, we secondly present experimental methods to assess bank strength effects that can be used in the design of river pattern experiments. The third issue is that riparian vegetation has often been represented in experiments by uniformly seeded sprouts of a single plant species, whilst spectacularly different patterns are obtained with contrasting seeding protocols, showing the need for other experimental procedures, and alternative riparian species. The main challenge for future experiments is better understanding of temporal scaling of biomorphodynamics.

1. Introduction

For more than a century, 'Giant' fluvial systems as found in nature have been miniaturized to 'Lilliputian' systems in the laboratory, so that workers could inspect the morphology and behaviour at close range with a known history, and within a short period (e.g., Reynolds, 1887; Yalin, 1971; Schumm et al., 1987). This experimental approach to the study of fluvial and deltaic morphodynamics lost some of its attraction in the second half of the last century with the advent of numerical models and increasing computing power. However, physical experiments and numerical models are not competitive but complementary pathways to the understanding of natural systems; and in recognition of this there is a revival of experimentation at the scale of landscapes (e.g., Paola et al., 2009; Kleinhans et al., 2014). In experiments we have full control over the initial and boundary conditions, and evolution is usually much more rapid than in the larger systems in nature. Experiments have advantages over numerical modelling, namely materiality: the physical, chemical, and biological materials, and processes at work in the experiment are real as in the natural world, unlike those in numerical models that are virtual (Morgan, 2003; Kleinhans et al., 2005). Numerical models, even if based on the laws of physics, depend on choices of the physics included, resolution, and other numerical issues related to discretization, and propagation of errors. On the other hand, numerical models are entirely repeatable, which allows study of variables in isolation, and scenario analyses (Oreskes et al., 1994; Kleinhans et al., 2005).

Recent progress in landscape experiments resulted in convincing morphological similarities between the experiments and natural systems, despite violation of some of the classical similarity scaling rules employed in civil engineering studies in the past. However, questions remain about the spatial and temporal scaling between nature and such experiments. Given sufficient similarity of physical and biological processes, physical experiments are not only scaled-down representations of larger systems but are rivers and deltas in their own right (e.g., Leopold and Wolman, 1957; Paola et al., 2009). Often relations

* Corresponding author.
E-mail address: m.g.kleinhans@uu.nl (M.G. Kleinhans).
URL: http://www.geo.uu.nl/fg/mkleinhans (M.G. Kleinhans).

http://dx.doi.org/10.1016/j.geomorph.2015.04.022
0169-555X/

exist between the spatial scale of a range of the phenomena in these landscapes and the typical time scales of development, but these relations change with the overall size of the system (Fig. 1). The landscape or reach scale is therefore defined relative to the largest phenomena of interest: as ranging between the length of individual river bars and bends, and the length of an entire valley or delta from apex to coastline. Here we focus on alluvial experiments where the bed and banks of experimental rivers are self-formed.

Many works in the past investigated and debated how closely experiments with very small rivers and deltas are comparable to large-scale natural systems. In the ideal situation the geometric scale of prototype relative to experiment would be valid for all three Cartesian dimensions, for the channel dimensions, gradient, particle size, and for the bar, and bend characteristics. However, it has long been clear that such perfect scaling is impossible for several reasons, not in the least that river bed sediment size reduced by the same scale would be cohesive sediment that has very different behaviour (e.g., Reynolds, 1887; Yalin, 1971; Schumm et al., 1987; de Vries et al., 1990; Hughes, 1993; Peakall et al., 1996; Cazanacli et al., 2002; Malverti et al., 2008; Paola et al., 2009; Kleinhans et al., 2014). Furthermore, the four variables slope, grain size, channel depth, and width can adjust independently during experiments and in the field. Regardless of the strict classical scaling rules it would appear that experiments that remain within certain thresholds, i.e., a relaxed scaling procedure, produce morphodynamics that are similar in size ratios, patterns, and dynamics to the larger-scale rivers and deltas found in nature (Paola et al., 2009; Kleinhans et al., 2014). In particular, self-formed experiments should have sediment of similar mobility. Additionally, these experiments should have subcritical to critical flow, a hydraulically rough bed, that is, particles on average larger than about 0.5 mm, and channel banks should be cohesionless to slightly cohesive or strengthened by vegetation such that banks are at least locally erodible, for reasons elaborated below.

Bank stability is important for channel pattern formation: the tendency to form alternate bars and meanders, and the degree of braiding strongly depend on the channel aspect ratio or the width to depth ratio. In turn, this ratio is mostly determined by bank strength, which is a function of a host of variables including the cohesive material strength, and vegetation cover (Fig. 3) (Ferguson, 1987; Eaton and Giles, 2009; Kleinhans, 2010). These properties should be scaled down in experiments as to remain in balance with the force exerted by the small-scale experimental flows. This makes real clay unusable (Schumm et al., 1987), but less cohesive substances have been used with success, such as silt-sized silica flour (van de Lageweg et al., 2013; W.M. Van Dijk et al., 2013), a polymer (Hoyal and Sheets, 2009) or polymer-rich substances such as corn starch (Smith, 1998). Rivers also tend to maintain a single thread if the floodplain does not offer suitable locations for local, and short-term channel incision, such as topographic lows in the floodplain or noncohesive patches that can easily be eroded. So, to fill these lows in the floodplain and hinder channel formation, and avulsion, specific sediments and vegetation have generally been used, in particular coal (Sheets et al., 2002), sand-sized low-density material (Braudrick et al., 2009) and seedlings of alfalfa (*Medicago sativa*, Fig. 1) (Gran and Paola, 2001; Braudrick et al., 2009; Tal and Paola, 2010). The latter also added strength to the banks (Tal and Paola, 2010; W. van Dijk et al., 2013). For further experimental design, a detailed auxiliary test setup for bank erosion has been used to quantify erosion rate of such strengthened experimental banks (Kleinhans et al., 2014). Clearly the spatial distribution of strength from cohesion and vegetation as well as floodplain filling on the floodplain affects the overall river pattern. This is supported at least qualitatively by bar and bend theory (review in Seminara, 2005), and by empirical work on vegetation in natural rivers (review in Gurnell et al., 2012).

This paper addresses three relatively new questions made possible by the experimental and theoretical progress in the past decade. On the basis of review, and new analysis, we first address the length scaling of bars and bends. This is followed by a review and discussion of the time scaling of experiments. Finally, the role of experimental vegetation in setting temporal and spatial scales is discussed and illustrated in a novel experimental setup. Below, we first develop these questions.

First, does bar *theory* predict scale effects in the sense that bar length and backwater adaptation length relative to channel width change as a function of scale (from experiments to large rivers)? We will consider this question with other conditions being equal, in particular the width–depth ratio of the channels and sediment mobility. In our earlier work we presented river and delta experiments, and a practical strategy to design such experiments, including application of bar theory (Kleinhans et al., 2014). Here we work from the opposite point of view: based on theoretical rivers ranging from 0.01 to 10,000 m in width we apply bar theory to study possible scale effects in river pattern.

Second, how can the *timescale* associated with bar pattern and bend migration be predicted? Morphology is created from spatial gradients in

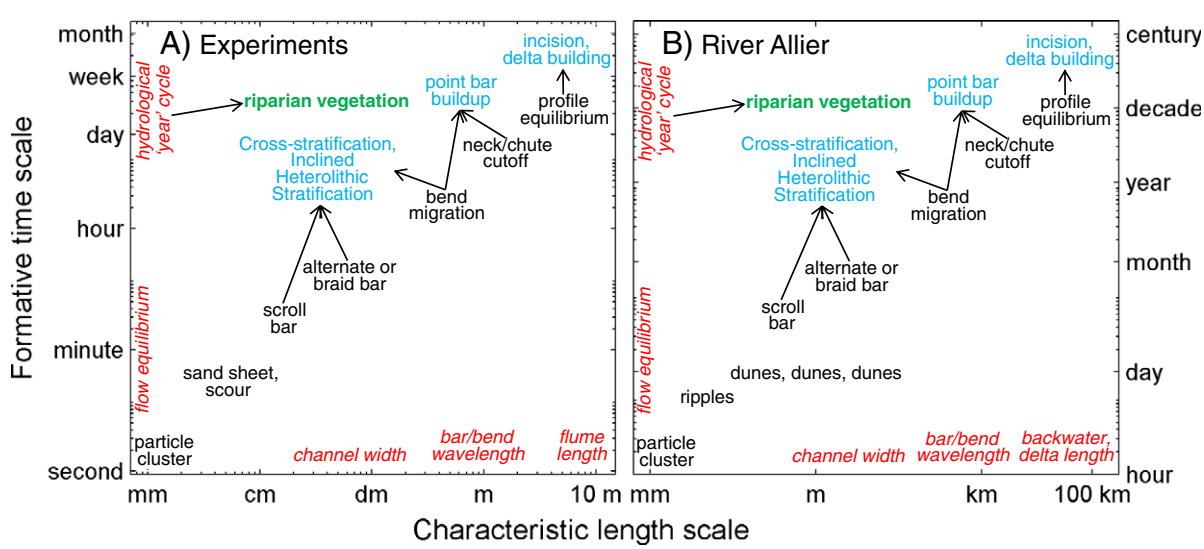

Fig. 1. Sketch of observed relations between characteristic spatial scale, and formative time scale for morphological phenomena relevant for self-formed river landscapes for (A) experiments discussed in this paper, and (B) the Allier river in France (Kleinhans and van den Berg, 2011). Red is indication of typical scales. Blue indicates stratigraphic elements at different scales that form because of morphodynamics at that scale. Vegetation is indicated in green.

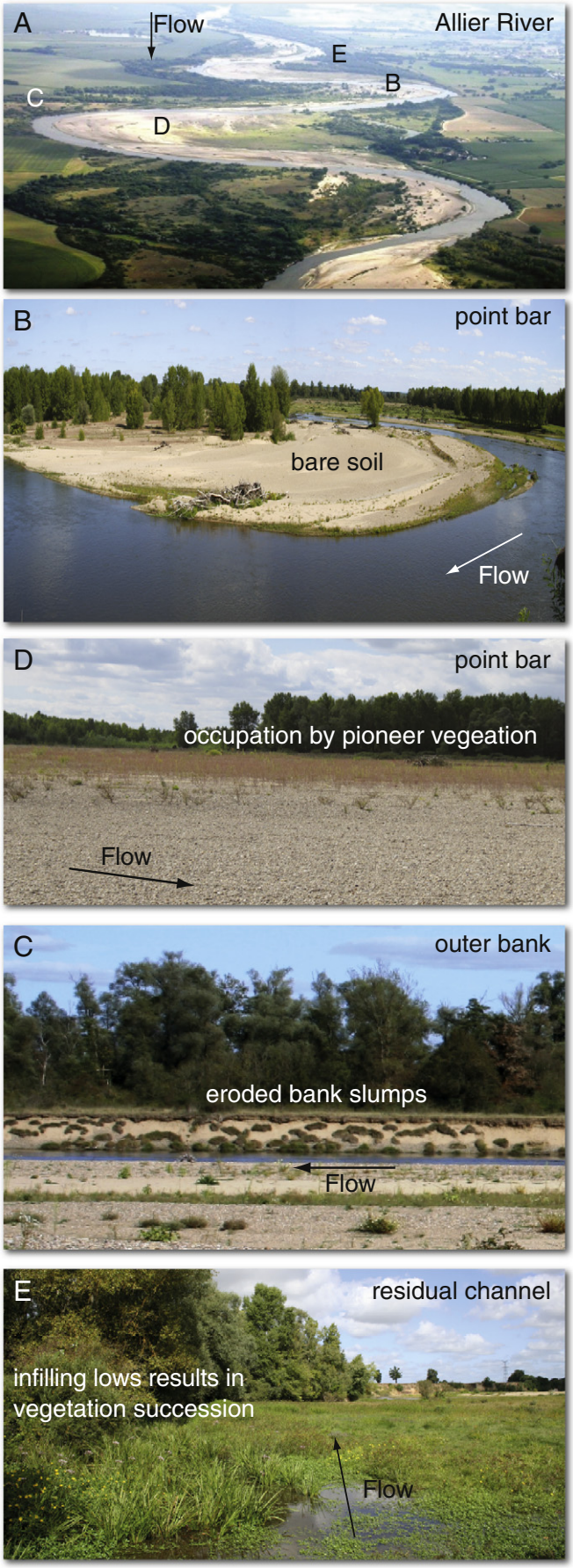

Fig. 2. Vegetation patches in a meandering gravel-bed river dominated by chutes. (A) Top view image showing vegetation patches in former channels, and succession, and locations for (B)–(E) along the Allier river in France (photo courtesy: Gertjan Geerling). (B) A point bar without vegetation that is often reoccupied by the river (Van Dijk et al., 2014). (C) Pioneer vegetation (Poplar) starting to establish during a period without extreme discharges. (D) Small slumps of vegetated blocks on the outer bank that may reduce the rate of bank erosion. (E) Vegetation in an abandoned channel enhances sediment capturing, which partly removes the floodplain lows, and allows development of other species requiring different substrates (Geerling et al., 2006).

sediment transport so that the transport rate is key to the time scale. A morphological time scale has therefore been based on sediment transport rates and gradients, and a relevant volume of sediment to be moved (de Vries et al., 1990). For the simplest case of delta building, where deltas are near-perfect traps of sediment, the transport gradient equals the transport magnitude. Thus a time scale follows from the total sediment feed rate divided by delta volume (M. van Dijk et al., 2012; de Villiers et al., 2013). However, how the time scale derived from bed sediment transport gradients would work for the building of relief within river plains, and whether this changes with spatial scale and bank strength, has not sufficiently been studied.

Third, which type of *riparian vegetation* does the alfalfa species represent in terms of settling rules, and how do the spatial and temporal distribution, and the growing conditions affect the river pattern? On the one hand a large number of riparian plant species exist, but on the other hand groups of species exist that have the same characteristics and fill the same niche in different regions and climate zones. Reported experiments perhaps represent different natural systems as the alfalfa was seeded in different ways, but perhaps we lack laboratory plant species for certain niches. These three questions will be addressed and discussed in the following three sections, which are followed by general conclusions.

2. The measure of experimental rivers

2.1. Outline: from similarity of channel geometry to scale effect analysis using bar theory

In this section we will use predictions from bar theory to assess whether scale effects are to be expected in bar length relative to channel width and in braiding index for landscape experiments of river patterns. We normalise the bar length to width not only because length depends on width, but also because the length scale of an experiment is most conveniently characterised by the scale of the channel width. The first step is to establish the minimum necessary conditions of flow and sediment mobility, which we summarise from earlier work and which deviate from those of classic similarity scaling. A more important and second step is a selection of semiempirical relations that predict channel geometry and flow conditions. Channel geometry is perhaps the most important variable in bar theory, but the most difficult to predict because it depends on floodplain characteristics. A test on experimental and field data is done to support the adequacy for the present purpose. In the third and final step we apply bar theory to a large range of channel dimensions, slopes, and particle sizes bracketing small experiments and the largest rivers on Earth. If there are no discernable scale effects then this provides physics-based support for the general claim that landscape experiments, strongly distorted in classical scaling terms, can be used quantitatively for river pattern studies.

As spatial gradients in sediment transport cause morphological change in the channel, it follows that larger morphological adjustments require more time. To illustrate this we plot a number of morphological phenomena on formative time scale and characteristic spatial scale in Fig. 1 for typical meandering and braiding experiments, and for the river Allier in France (Kleinhans and van den Berg, 2011; W.M. Van Dijk et al., 2012). Here we regard (point) bars and related vegetation patches as the larger-scale elements of braided and meandering rivers.

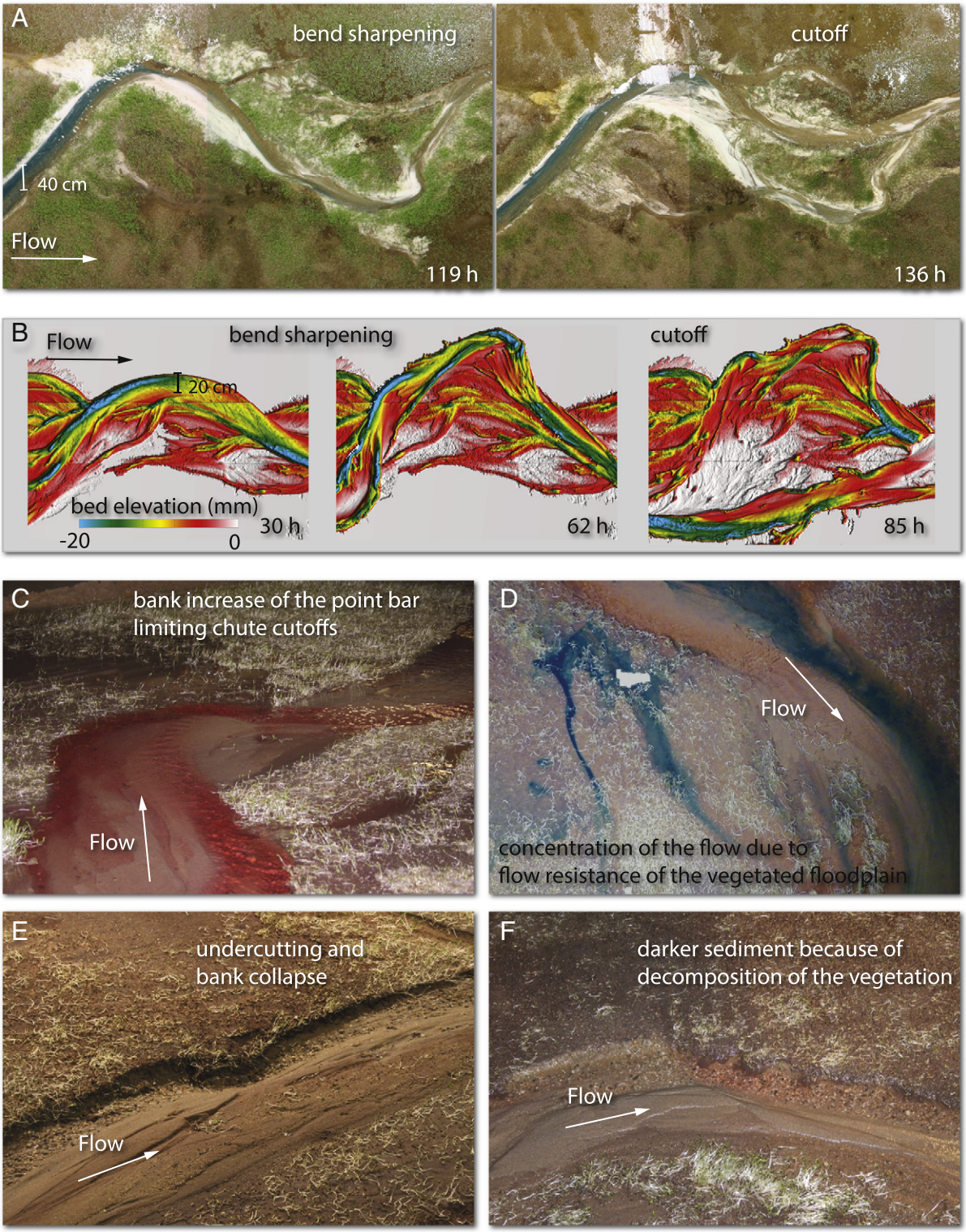

Fig. 3. Overview of vegetation effect in experimental meandering rivers. (A, B) Uniformly seeded floodplain shows bend sharpening because of strong, vegetated outer banks. Afterward, overbank flow increased on the point bar so that later the bend was cut off in the experiments of Braudrick et al. (2009, (A)), and W. van Dijk et al. (2013, (B–F)). (C) Vegetation on the inner-bank point bar increases flow resistance, and bank strength, so that chute cutoff frequency reduces. (D) Overbank flow is concentrated between less dense vegetation patches on the floodplain. (E) An undercut, vegetated bank collapsed, and protected the bank against further erosion. (F) The vegetated floodplain shows darker colours from decomposed alfalfa seeds, which probably enhanced bank cohesion.

These are further populated by smaller-scale elements such as chute cutoff channels and small bars. With the focus on channel and bar patterns in mind, even smaller-scale phenomena such as individual particle clusters, scours, and bedforms can be seen as noise on that larger scale, whereas the profile of a valley or delta can be seen as an external forcing on the morphodynamic phenomena of interest here.

A striking difference between laboratory experiments and full-scale rivers is that the latter exhibit multiple scales of bedforms that are not

found in experiments, in particular ripples and dunes that occur in subcritical flow with mobile bed sediment in gravel- and sand-bed rivers. Unlike bars, which scale with channel width, bedforms scale approximately with water depth. Apparently these bedforms are not necessary to form the larger-scale morphological features of rivers despite their known effects on flow resistance, sediment transport and sorting, and stratigraphy. Although this question merits further research, the tentative assumption that bedforms are irrelevant for river patterns is supported by the fact that bedforms are also not part of numerical morphological models, except indirectly as uniform flow resistance, whilst the even smaller-scale process of sediment transport is essential (e.g., Schuurman et al., 2013). We speculate that bedforms and larger-scale morphology are caused by the same underlying physical processes and that bedforms are not a cause for larger-scale morphology. Therefore the remainder of this paper will concentrate on bars and bends as a characteristic dimension of the pattern of a river. To predict these, typical channel dimensions are required as explained below.

Prediction of bar wavelengths from linear theory works moderately well for natural rivers, and is in general agreement with empirical channel pattern stability diagrams (Kleinhans and van den Berg, 2011). These depend strongly on channel aspect ratio, and therefore indirectly on channel bank, and floodplain strength (Kleinhans, 2010). Here, width and depth are defined at a channel-forming discharge, for instance the bankfull discharge or the mean annual flood (Kleinhans and van den Berg, 2011). However, in order to use such predictors the channel width, depth, gradient, and particle size must be known in advance. This is a key problem in experimental design (Kleinhans et al., 2014). Here we first describe the theory with which to predict bar length and braiding index, and then resolve the hydraulic geometry problem in two alternative ways: i) an empirical fit to field and experimental data, and ii) the quasi-universal bankfull relations of Parker et al. (2007) from which we then predict bar pattern properties.

We illustrate the results of the analyses with data of natural gravel-bed rivers from the data set of Kleinhans and van den Berg (2011), summary conditions for experiments listed in Table 1 (Kleinhans et al., 2014), and additional experimental data of Fujita (1989), and Egozi and Ashmore (2008). The latter two contain experimental braided rivers with a large range of conditions and degree of braiding but represent different aspects of the braiding: the Egozi and Ashmore (2008) data refer to individual channels within a braid plain, whereas the Fujita (1989) data refer to the entire braid plain (where the width is equal to the flume width) with multiple bars and channels. The Fujita (1989) experiments are not truly alluvial in that the channel abuts the flume walls but are shown here because they successfully formed braided river bar patterns. The experimental summary data taken from Kleinhans et al. (2014) also contain meandering rivers and delta experiments, and have a much wider range in particle size and mobility.

2.2. Review of experimental scaling by dimensionless flow and sediment mobility

A number of reviews dealt in detail with various schools of scaling (e.g., Reynolds, 1887; Yalin, 1971; Schumm et al., 1987; de Vries et al., 1990; Hughes, 1993; Peakall et al., 1996; Cazanacli et al., 2002; Maynord, 2006; Malverti et al., 2008; Paola et al., 2009). Here we limit the overview to the most essential variables identified in Kleinhans et al. (2014) and related works and show that an extra closure relation is needed for the additional degree of freedom of self-formed channel width.

The Froude number is the ratio of flow velocity and shallow water wave celerity, and determines the interaction of the water surface with the bed:

$$Fr = \frac{u}{\sqrt{gh}} \tag{1}$$

where u = cross-sectionally averaged flow velocity, h = width-averaged water depth and g = gravitational acceleration. In alluvial experiments, this number should generally remain below unity.

The key issue in reproducing mobile bed morphology and resultant stratigraphy is sediment mobility, expressed in the form of the Shields number (θ):

$$\theta = \frac{\tau}{\left(\rho_s - \rho_f\right) g D_{50}} \tag{2}$$

where in steady uniform flow, $\tau = \rho_f g h \sin S \approx \rho_f g h S$ is the total shear stress, with ρ_f = density of fluid, ρ_s = density of sediment, and D = particle diameter, usually the mean or median of the distribution by weight. When the Chezy law $u = C\sqrt{hS}$ is inserted, shear stress can also be expressed as

$$\tau = \rho_f g \frac{u^2}{C^2} \tag{3}$$

Table 1
Dimensional, and dimensionless characteristics of selected river, and delta experiments reported in Friedkin (1945), Schumm and Khan (1972), Egozi and Ashmore (2009), Smith (1998), Peakall et al. (2007), Braudrick et al. (2009), Tal and Paola (2010), W.M. Van Dijk et al. (2012, 2013), Sheets et al. (2002), and Hoyal and Sheets (2009), and taken from Kleinhans et al. (2014).

Variable		Friedkin	Schumm	Ashmore	Smith	Peakall	Braudrick	Tal	v Dijk 1	v Dijk 2	Sheets	Hoyal	Unit	Eq.
Discharge	Q	1.42	4.25	2.8	0.71	0.51	1.8	2	1	0.3	0.5	0.33	10^{-3} m^3/s	–
Slope	S	0.0075	0.02	0.015	0.015	0.008	0.0046	0.015	0.0055	0.01	0.05	NA	m/m	–
Particle size	D_{10}	0.2	0.2	0.25	0.01	0.12	0.62	0.3	0.25	0.25	0.12	0.005	10^{-3} m	–
Particle size	D_{50}	1.2	0.7	1.2	0.03	0.21	0.8	0.5	0.51	0.51	0.12	0.05	10^{-3} m	–
Particle size	D_{90}	3	1.2	3.6	0.05	1.03	1.04	0.7	1.35	1.35	0.12	0.45	10^{-3} m	–
Channel width	W	0.23	0.671	1.15	0.04	0.116	0.4	0.4	0.3	0.15	0.115	0.05	m	–
Channel depth	h	0.0457	0.0762	0.009	0.005	0.015	0.013	0.02	0.015	0.010	0.028	0.023	m	–
Froude number	Fr	0.19	0.10	0.91	0.90	0.76	0.87	0.56	0.78	0.80	0.30	0.59	–	(1)
Backwater length	λ_{bw}	18.3	114.3	1.8	1.0	5.6	8.5	4.0	8.2	3.0	1.65	15.1	m	(20)
Reynolds number	Re	5800	6400	2400	1000	4400	4100	5000	4500	2500	4400	6600	–	
Weber number	We	10.1	7.3	9.0	2.7	17.6	17.3	17.1	18.5	8.6	9.4	25.7	–	
Reynolds* number	Re^*	174.0	46.4	131	1.4	35.3	25.2	38.0	45.9	45.9	34.8	0.16	–	
Shields number	θ	0.17	0.13	0.07	1.52	0.35	0.05	0.36	0.10	0.12	6.94	0.14	–	(2)
Chezy number	C	40.7	51.9	26.6	55.5	40.4	39.2	45.6	38.3	35.1	54.7	85.4	m$^{1/2}$/s	(4)
Sed. tr. nonlinearity	n	10	10	10	4	10	10	10	10	10	4	10	–	See (5)
Bar length	Lp	0.64	1.51	–	1.78	–	5.34	2.37	3.95	1.52	0.77	–	m	(5)
Damping length	Ld	−0.38	−0.28	−0.29	0.19	0.26	11.4	−0.28	2.04	1.02	−0.38	0.014	m	
Interaction param.	IP	0.43	1.02	13.29	0.30	0.30	0.26	1.96	0.20	0.21	4.28	0.004	–	
Braiding index	B_i	1.36	1.83	5.29	1.0	1.0	1.17	2.34	1.17	1.17	1.53	1.0	–	(9)

where the Colebrook–White relation describes the dependence of the Chezy number on water depth and characteristic friction length k_s

$$C_b = 18 \log \frac{12h}{k_s} \tag{4}$$

where $k_s = D_{90}$ in the case of skin friction C', grain-related shear stress τ' and mobility θ'. This incidentally shows that the problem of a priori estimation of channel slope and friction are related problems requiring one closure relation (e.g., Eke et al., 2014). Note however that a representation of sediment mobility of a channel by a single number ignores that channel depth is strongly variable (Ashmore, 1982; Bertoldi et al., 2009).

Furthermore, a single Shields number ignores the complexity of sediment sorting effects on mobility (Wilcock and McArdell, 1997; Gardner and Ashmore, 2011). Few indications exist that the sorting patterns formed in experimental braided and meandering rivers are similar to those in natural gravel-bed rivers (Leddy et al., 1993; Pyrce and Ashmore, 2005; Gardner and Ashmore, 2011; van de Lageweg et al., 2014). Also sorting patterns in finer-grained systems such as experimental analogues for gravel-bed meandering rivers with floodplains (W.M. Van Dijk et al., 2013), and fine-grained deltas simulated with low-density sediment and polymer (Hoyal and Sheets, 2009) resemble those in natural systems in important respects. Clearly this potential of studying sorting patterns has not fully been explored yet, and consequently detailed comparisons with sorting trends in nature are lacking.

Most importantly, a solution to the above equations from boundary conditions flow discharge, sediment supply, particle size, and gradient requires that width is known. However, channel width is the result of several processes that form and modify river channels. Until now, hydraulic geometry relations of varying complexity have been used to resolve this, pending further development of constitutive relations that include the properties of the floodplain such as material strength and vegetation rooting (e.g., Eaton and Church, 2007). Later we will adopt simpler relations for the sake of isolating the effect of channel size on bar pattern without bank strength and vegetation effects.

2.3. Theory for bar wavelength and braiding index

Given an acceptable similarity of flow and sediment mobility, we now turn to the similarity of bars and meandering channels. Here we show that useful theory exists for such predictions, which depends strongly on hydraulic geometry to which we turn in the next section. The wavelength of channels and bars can be predicted from perturbation analysis after linearising the theoretical relations for flow, sediment transport and morphology (Struiksma et al., 1985). Dimensionless bar period (or wavelength) L_p is calculated from

$$\frac{2\pi\lambda_w}{L_p} = \frac{1}{2}\sqrt{(n+1)\frac{\lambda_w}{\lambda_s} - \left(\frac{\lambda_w}{\lambda_s}\right)^2 - \left(\frac{n-3}{2}\right)^2} \tag{5}$$

Here n = the degree of nonlinearity of sediment transport dependence on depth-averaged flow velocity ($q_b = f(u^n)$). For a classical bedload transport predictor such as that of Meyer-Peter and Mueller (1948), $n \geq 3$ for high Shields numbers, and increases to infinity toward the critical Shields number for sediment motion. We use $n = 10$, which applies to gravel-bed rivers (following Crosato and Mosselman, 2009). The adaptation length λ_w (m) of transverse flow is given as

$$\lambda_w = \frac{C^2 h}{2g} \tag{6}$$

and the adaptation length of a bed disturbance λ_s (m) is calculated as

$$\lambda_s = \frac{h}{\pi^2}\left(\frac{W}{h}\right)^2 f(\theta) \tag{7}$$

where W is channel width (m), and where the magnitude of the transverse slope effect $f(\theta)$ represents the direct effect of gravity on particles moving on a transverse slope (Ikeda, 1982):

$$f(\theta) = \alpha_\theta \sqrt{\theta} \tag{8}$$

where α_θ is calculated from a constitutive relation (Talmon et al., 1995). The resonant bar length is the minimum calculated for a range of channel aspect ratios in otherwise constant conditions, and can be thought of as the optimal meander bend length.

A complementary descriptor of the bar pattern is the number of active channels given as a braiding index B_i. Crosato and Mosselman (2009) derived an analytical braiding index predictor building on the theory of Struiksma et al. (1985) for sand- and gravel-bed rivers:

$$B_i = \frac{1}{2}\left[\sqrt{\frac{0.17g(n-3)}{\sqrt{\frac{\rho_s-\rho_f}{\rho_f}D_{50}}}\frac{W^3 S}{CQ}} - 1\right] + 1. \tag{9}$$

Clearly, the predictive relations reviewed above would be very useful, but they are strongly dependent on channel geometry, which is unknown in most cases.

2.4. Hydraulic geometry relations for Lilliput- to Giant-sized channels

The aim in this section is to universally assess effects of the size of a river on bar pattern, in particular bar length relative to channel width. We will identify possible scale effects by application of physics-based bar theory to the experimental and the natural scales, from which scale effects could emerge as we have to fulfil several requirements at the same time, including the necessary channel geometry, sediment mobility, and realistic friction. This is because prediction of a bar length, resonant bar length and braiding index requires an estimate of the bankfull channel geometry, slope, and particle size. Bankfull geometry in experiments depends strongly on floodplain formation processes, for which we have no theory with practical applicability in experiments. However, it is possible to do auxiliary experiments to assess the amount of cohesive material and vegetation necessary to obtain channel geometry that results in the required channel pattern (Kleinhans et al., 2014).

Below we will predict bar length and braiding index for a set of rivers with scales ranging from the smallest experiment to the largest river on Earth. In order to do so, a set of relations to calculate channel dimensions, gradient, and particle size is needed rather than a data set. Here we present two complementary sets of relations to bracket the uncertainty related to the closures for hydraulic resistance and bank strength. The first ad hoc set of relations is fitted to some experimental and field data. These are intended solely for descriptive use and scenario prediction of bar characteristics in this paper. The second is an internally consistent and complete set of relations for predicting bankfull channel geometry, slope, and characteristic sediment size (Parker et al., 2007). In both sets the slope predictor is rather uncertain which has a large effect on predicted bar pattern.

2.4.1. Hydraulic geometry with imposed channel aspect ratio

We first defined a typical channel aspect ratio, and, to define the scale of a range of rivers, a range of channel widths, from which we calculated depth. We then repeated the exercise for a range of aspect ratios that we applied to all previously defined depths to calculate an additional range of rivers. For a typical channel aspect ratio W/h =

30, we chose an arbitrary hydraulic geometry relation for width that is empirically adequate for the field data of Kleinhans and van den Berg (2011):

$$W_e = 6Q^{0.41}. \tag{10}$$

The discharge in channels with different aspect ratios is set proportional to the different width so that, given the same depth but a different width, the flow velocity in channels of the same scale but different aspect ratios remains the same. This allows calculation of the Froude number and of the product $C\sqrt{S} = u/\sqrt{h}$.

To solve C and S we use a broad-brush empirical relation $S = f(Q)$ that predicts slopes typically found in natural rivers:

$$S = 0.01Q^{-0.05} \tag{11}$$

which implicitly is a friction relation.

The final unknown particle size D is calculated under the assumption of a constant bankfull Shields mobility number $\theta_{bf} = 0.05$, which is larger than the critical Shields number for sediment motion $\theta_{bf} = 0.03$, and typical for bankfull flow conditions in braided gravel-bed rivers (Parker et al., 2007).

2.4.2. Quasi-universal hydraulic geometry with bank strength parameter

Parker et al. (2007) developed a set of relations for predicting bankfull channel geometry, slope, and characteristic sediment size that is internally consistent and complete. Empirical coefficients in these relations were calibrated on a data set of gravel-bed rivers from three regions on Earth with discharge ranging from $2.7 < Q < 5440$ m^3/s and median sediment sizes from $0.027 < D < 0.168$ m. Further constitutive relations were involved to complete the set: the Manning–Strickler relation for flow resistance, a bankfull Shields mobility number characteristic for gravel-bed rivers, and a sediment transport relation, in this case the Parker approximation to the Einstein function.

Particle size is now related directly to discharge through the definition of dimensionless discharge (Parker et al., 2007):

$$D = \left(\frac{Q}{\sqrt{g}Q_c}\right)^{2/5} \tag{12}$$

which we solved for a range of Q, a channel aspect ratio of 30, and an arbitrary dimensionless $Q_c = 20,000$, which results in reasonable particle sizes for gravel-bed rivers as shown later.

Using the grain sizes from the previous equation, channel width is predicted from (Parker et al., 2007):

$$W_p = \frac{\alpha_W}{g^{1/5}} Q^{2/5} \left(\frac{Q}{\sqrt{g}D^{5/2}}\right)^{n_W} \tag{13}$$

where

$$\alpha_W = \frac{0.0033}{\sqrt{\frac{\rho_s - \rho_f}{\rho_f} 11.2\left(1-\frac{1}{r}\right)^{4.5}(0.0143r)^{3/2}}} \tag{14}$$

and

$$n_W = \frac{1}{5} - \frac{1}{2}\cdot 0.0561 - \frac{2}{5}\cdot 0.263 \tag{15}$$

where the original empirical constants of Parker et al. (2007) are retained for clarity. Here the parameter $r = \theta_{bf}/\theta_c$ is a surrogate for bank strength, which we choose here as a range of values between $4/3 < r < 2$ to create a range of rivers with different channel aspect ratios.

Water depth is predicted from Parker et al. (2007):

$$h = \frac{1}{g^{1/5}} Q^{2/5} \left[\frac{11.2\left(1-\frac{1}{r}\right)^{4.5} 0.0143r}{0.0033\cdot 3.71}\right]^{\frac{1}{1+0.263}}. \tag{16}$$

The channel slope is predicted from Parker et al. (2007):

$$S = \alpha_S \left(\frac{Q}{\sqrt{g}D^{5/2}}\right)^{n_S} \tag{17}$$

where

$$\alpha_S = 0.0143\left(\frac{\rho_s - \rho_f}{\rho_f}\right)\left[\frac{11.2\left(1-\frac{1}{r}\right)^{4.5} 0.0143r}{0.0033\cdot 3.71}\right]^{\frac{1}{1+0.263}} \tag{18}$$

and

$$n_S = \frac{2}{5} - 0.0561. \tag{19}$$

2.5. Comparison of scales of experiments and natural rivers

2.5.1. Channel dimensions, slope, and particle size as a function of scale

We will now create a consistent space of hydraulic geometry values to use in the bar theory calculations. The two aforementioned sets of semiempirical relations for channel geometry were therefore applied to a large range of scales, and a large range of channel aspect ratios, and compared to field and experimental data (Figs. 4 and 5). Channel geometry was then plotted in the dimensionless form of Parker et al. (2007) against dimensional discharge so that the scale of the river became clear (Fig. 4).

The empirical and Parker predictors are quite close for width and depth, and show the required dependence on specified channel aspect ratio (or bank stability surrogate r). The data show similar trends for experiments and for natural rivers, with dimensionless width increasing with discharge and dimensionless depth decreasing as discharge increases. A larger proportion of slopes from the Kleinhans and van den Berg (2011) data set have slopes < 0.005, which is steeper than the experimental slopes. The empirical relation overpredicts the slope of many rivers in the field, but does a reasonable job of predicting slope in the laboratory. In contrast, the Parker et al. (2007) relation reasonably predicts slopes for the field data set, but underpredicts experimental slopes by about an order of magnitude. The underprediction of slope occurs for a range of values of Q_c. This may occur because the requirements for laboratory experiments outlined in the introduction are not compatible with scaling using Parker et al. (2007) and because of the strong dependence of Q_c on D_{50}; small differences in scaling D_{50}, and discharge can result in very large differences in predicted slope. The Parker et al. (2007) relation was developed for gravel-bed rivers, and although the relationships are dimensionless, extending the relationships to the laboratory where gravel-bed rivers are often scaled down to sandy beds may not be appropriate. Additionally, predicted slope is insensitive to channel aspect ratio for the empirical predictor, and somewhat sensitive to the Parker et al. (2007) predictor, but the data show no discernable trend. The slope predictor of Parker et al. (2007, Eq. (17)) appears inadequate to predict the hydraulic geometry of the experiments.

Dimensional water depth and width are nearly the same for the empirical and Parker et al. (2007) relations (Fig. 5), and, for a large range of channel aspect ratios, approach the range of values observed in experiments and in nature. Likewise, flow velocity is fairly well bracketed, where the empirical relations show a slightly slower increase with scale than the Parker et al. (2007) relations. The particle size derived from the relations is fairly well recovered for the entire scale range.

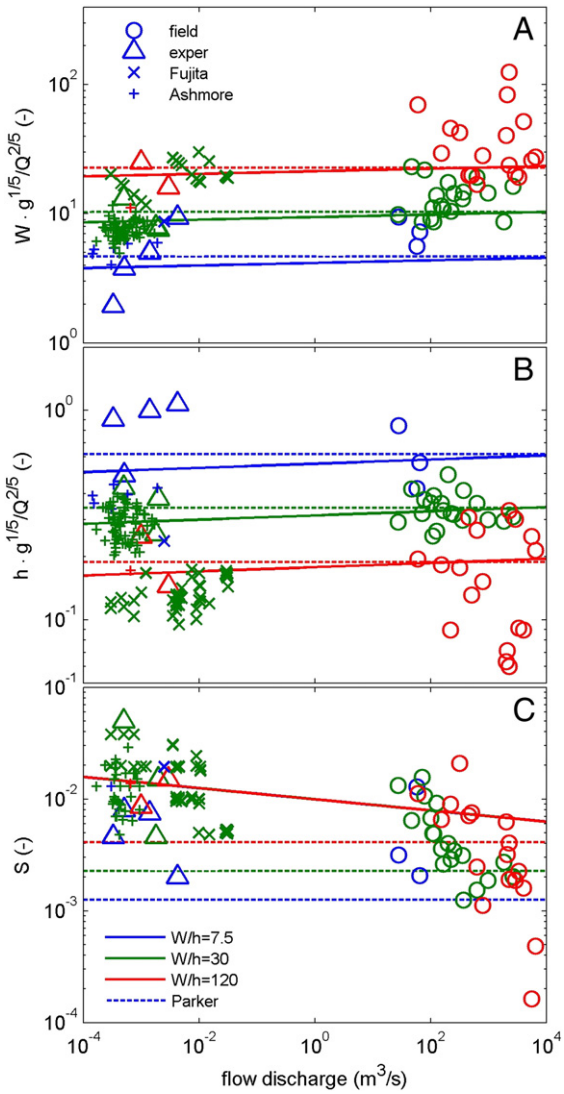

Fig. 4. Dimensionless channel dimensions, and slope as a function of dimensional flow discharge. The legends for symbology, and colours (indicating channel aspect ratio) apply to all panels.

The rate of increase of particle size by the empirical relations is close to observed, but values are somewhat larger; whereas the values from the Parker et al. (2007) relations are in closer agreement with the observations, but the rate of increase is somewhat larger than observed. Note however that the present data include rivers with very fine gravel not included in the calibration of the Parker et al. (2007) relations.

The Chezy flow resistance parameter resulting from the empirical predictors of channel dimensions and slope is about 20, constant for the entire scale range, and hardly dependent on channel aspect ratio. The Chezy numbers resulting from the Parker et al. (2007) relations plot a bit higher, and show a weak dependence on channel aspect ratio. The data scatter more than an order of magnitude below and above the predictions, which is not surprising given the large variety of river patterns and conditions included in the data. The predicted Froude numbers are also insensitive to channel aspect ratio, and plot below unity as expected (Grant, 1997). Data scatter can be caused by natural variations in conditions, measurement error, and the fact that highly heterogeneous cross sections are summarised in one value. Hence the experimental data plotting up to $Fr < 2$ need not have been beyond critical and include the Fujita cases with fixed flume walls. The 'predicted' Shields mobility numbers were a priori set at a low number, but vary strongly in the experiments and field data because the sediment may be finer than coarse gravel in rivers, and in experiments the sediment may be finer sand.

So far, these results show that sand-bed rivers in the laboratory often scale in channel dimensions, slope, and bed material size as gravel-bed rivers in nature, which are generally close to the beginning of sediment motion at bankfull flow conditions. Furthermore, the most important dimensionless quantities, the Froude, and Shields numbers, are generally similar except for braided channels with fixed sidewalls that constrain lateral channel migration as in the experiments of Fujita (1989). These results are the intermediate step toward the assessment of scale effects in bar length and braiding index to be predicted with bar theory in the next section.

2.5.2. Bar characteristics as a function of scale

To investigate the effect of channel scale, bar characteristics were calculated for a large range of channel dimensions, slopes, and particle sizes from the broad-brush relations evaluated above. An important length scale for flow over bars, bar and bend cutoff processes, and downstream control is the backwater adaptation length (Fig. 6A) (Ribberink and Van der Sande, 1985; Parker, 2004), which can be estimated as

$$\lambda_{bw} = \frac{h}{3S} \tag{20}$$

with $S =$ energy slope. The value calculated with this relation estimates the upstream distance over which the difference of water level between normal flow, and the backwater has decreased to 95% of the value at the point of origin. This number decreases rapidly for subcritical flow conditions. The backwater adaptation length is sensitive to channel aspect ratio because of the water depth. For the empirical relations this length reduces with smaller scales, but not nearly as strongly as for the observations. However, for the Parker et al. (2007) relations the backwater adaptation length appears independent of scale, which is largely the result of the under-prediction of channel slope (Fig. 4C). Note, however, that the backwater adaptation length calculation is not valid for nearly critical to supercritical flow, and numbers of backwater length relative to channel width below unity can be disregarded.

The bar characteristics are quite sensitive to the assumptions and different relations (Fig. 6B, C). The degree of braiding appears independent of scale, but the precise dependence on channel aspect ratio differs for the two sets of relations. Likewise, the resonant bar length is nearly independent of scale (Fig. 6B, C). This analysis indicates that scale effects are insignificant in the sense that the bar length relative to channel width or degree of braiding changes with the size of the river. This is under the assumption that the empirical and Parker et al. (2007) relations are valid, which appears to be supported by the data. However, the uncertainty of these relations is large because of the underlying uncertainty of hydraulic resistance and bank stability, so that it is conceivable that scale effects appear when more sensitive and accurate hydraulic geometry models are developed in the future. Nevertheless these findings agree in general with empirical relations that show linear scaling of bar spacing with 4–5 times the channel width (e.g., Hundey and Ashmore, 2009). In conclusion, this means that scale effects are absent, so that the bar pattern and bar length relative to channel width in experiments should be the same as that in nature if the channel geometry is the same, which can be tuned experimentally by floodplain formation processes.

3. Time scaling

3.1. Time scaling by Froude scaling

The time scale to form bars has hardly been studied in its own right in the laboratory and in models. Classical similarity scaling proceeds from geometrical similarity, flow, and sediment transport to a time

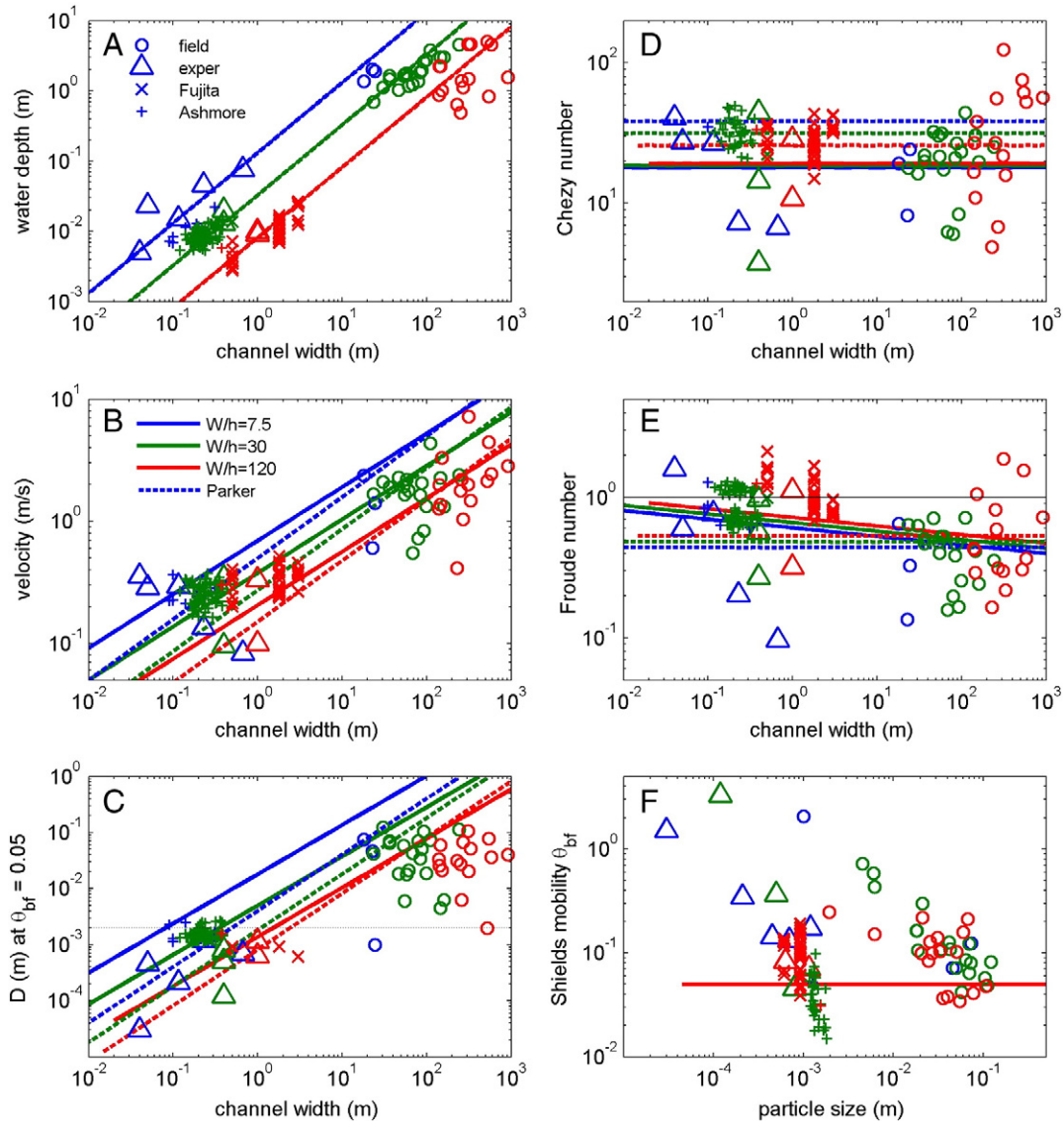

Fig. 5. Dimensional variables, and dimensionless parameters resulting from the empirical, and Parker et al. (2007) relations for channel dimensions, slope, and particle size in comparison to field data (Kleinhans and van den Berg, 2011), collected experiments (Table 1), and experimental data of Fujita (1989), and Egozi and Ashmore (pers. comm., 2008). The legends for symbology, and colours (indicating channel aspect ratio) apply to all panels.

scale of morphological change that is basically calculated from a volume divided by a sediment transport. This time scale is the same as that of the flow in the case of undistorted models; a condition called dynamic similarity (Yalin, 1971; de Vries et al., 1990). However, most landscape experiments that represent either larger or finer-grained systems than reaches of coarse gravel-bed rivers are distorted, meaning that the depth scale is larger than the horizontal length scale (Yalin, 1971). Moreover, important aspects of morphological change do not proceed from sediment transport alone but also from bank failure when cohesive or vegetated floodplains exist. To what degree bank failure processes set the bank migration rate rather than sediment transport that undercuts the banks remains an unanswered question. Here we review and compare classical and more recent analyses reported in the literature.

Laboratory channels are often scaled in spatial dimensions to prototypes in nature by flow and sediment mobility parameters as described earlier. This approach can be pursued further to scale time, assuming that the Froude number in the laboratory and the field are similar (Yalin, 1971; Struiksma, 1986; Braudrick et al., 2009). In Froude similarity, length scales in the laboratory channel are scaled to the field using a scaling factor σ defined as

$$L_{nature} = \sigma L_{lab} \tag{21}$$

where L_{lab} and L_{nature} are scales in the field and laboratory, respectively, representing any length scale such as channel width, channel depth, and grain diameter (Yalin, 1971; Struiksma, 1986; Braudrick et al., 2009). Distortion m is then defined such that $\sigma_h = m\sigma_L$, where typically the depth scale exceeds the horizontal length scale so that $m > 1$. The experiments described in Table 1 are not scaled directly from a particular river but from gravel-bed rivers in general. Laboratory rivers often scale as gravel-bed rivers, which gives σ between 25 and 100, depending on the parameter of interest, and the size of the flume.

Assuming Froude number similarity, we equate the Froude numbers in the laboratory and in nature:

$$\frac{u_{nature}}{gh_{nature}} = \frac{u_{lab}}{gh_{lab}}. \tag{22}$$

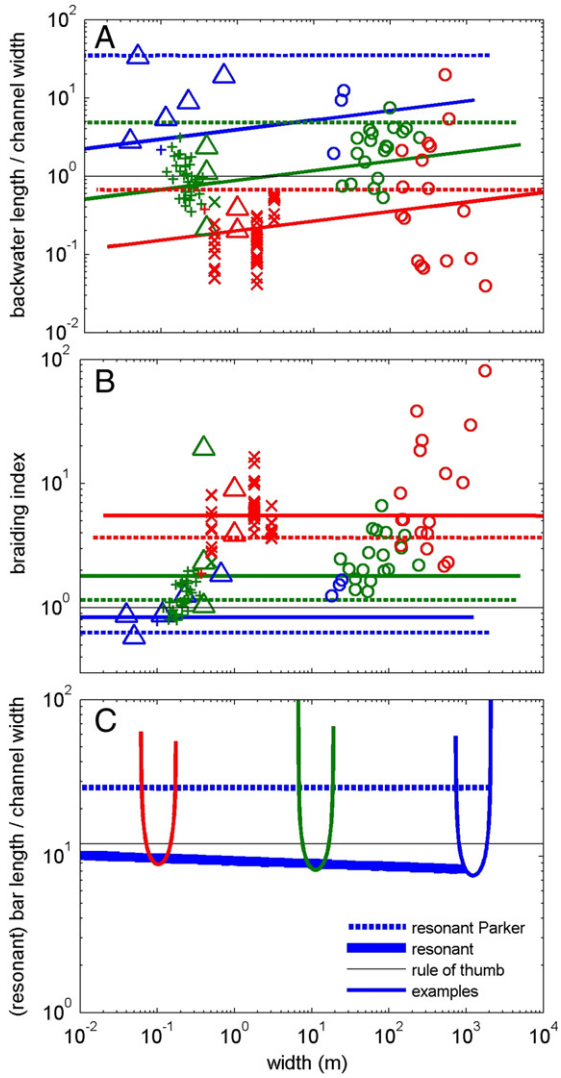

Fig. 6. Length scales predicted for a large-scale range of rivers, here represented by channel width, and for specific field, and laboratory conditions. (A) Relative backwater adaptation length. (B) Degree of braiding. Legends in (A), and (B) are the same as in Fig. 5. C. Relative bar length. Bold lines indicate the resonant bar length. The rule of thumb is bar length $\approx 12W$. The parabolas indicate bar lengths as a function of channel aspect ratio for one specific river discharge. The smallest, resonant bar length from all parabolas are given as the drawn line, which is nearly independent of river size indicated by channel width.

Because gravity is constant, and because depth is assumed to scale like the horizontal length scale, we can substitute $h_{nature} = \sigma h_{lab}$ to obtain

$$\frac{u_{nature}}{u_{lab}} = \sqrt{\sigma}. \tag{23}$$

Because velocity is a length scale divided by time,

$$\frac{T_{nature}}{T_{lab}} = \frac{\sigma}{\sqrt{\sigma}} = \sqrt{\sigma}. \tag{24}$$

A similar derivation was presented elsewhere (e.g., Klaven and Kopaliani, 1980; Eq. (9) in Shvidchenko and Kopaliani (1998). Natural gravel-bed rivers have long low-flow periods where the channel is not active, whereas laboratory rivers are usually in a state of perpetual flooding. This is quantified using an intermittency factor I (Parker et al., 1998; Braudrick et al., 2009):

$$\frac{T_{nature}}{T_{lab}} = \frac{\sqrt{\sigma}}{I}. \tag{25}$$

With this method, Braudrick et al. (2009) found that their migration rates corresponded to 0.5–0.8 channel widths per year, which is much faster than those observed in the field. However, the time scale derived above is basically a flow time scale, which perhaps differs from the time scale of sediment transport. To seek an explanation we will now discuss various other times scales for sediment transport found in literature.

3.2. Time scaling by sediment transport rate and characteristic volume

The one-dimensional time scale of adaptation of the longitudinal river bed profile over a length equal to the backwater adaptation length depends on the celerity of a bed defect. Furthermore, the migration celerity of a bed disturbance, for instance in the bar pattern, is the same as this bed defect as also demonstrated in a comparison with numerically modelled braid bars (Schuurman, 2015). The celerity is estimated as (Ribberink and Van der Sande, 1985)

$$c_b = \frac{dq_s}{dz} = \frac{nq_s}{h} \tag{26}$$

(in m/s) where the right approximation is in the limit of small bed defect heights dz. The adaptation time scale, here extended with intermittency, is then calculated as

$$T_{bw} = \frac{\lambda_{bw}}{Ic_b}. \tag{27}$$

The time scale predicted here concerns the propagation through a braided river of a perturbation, including the front of bars forming in the downstream direction on an initially plane bed in experiments or models (Schuurman, 2015). However, this is much faster than the migration of entire bars, and is therefore not suitable for the prediction of a time scale relevant for a comparison between fully developed bars in a river and an experiment.

A characteristic morphological time scale T can be calculated directly from the average sediment transport rate integrated over channel width Q_s, and a control volume V that is eroded or deposited (Yalin, 1971; de Vries et al., 1990):

$$T = \frac{V}{Q_s}. \tag{28}$$

As compared with the hydrodynamic time scale derived from Froude scaling, this now brings in explicitly the sediment transport. For deltas, the transport rate is simply the sediment feed rate and the volume is that of the entire delta, and the resulting time scale is the true time scale. For longitudinal adjustment of river channel profiles the sediment input is not completely trapped because the control volume of a reach also loses sediment at the downstream boundary. This means that a river channel profile adjusts by (exponential) relaxation to the equilibrium gradient, where the initial storage of sediment transport, calculated from the spatial gradient, determines a characteristic time scale after which about 63% of the total adjustment has been accomplished (Ribberink and Van der Sande, 1985; Parker, 2004).

On the basis of a time scale for grain motion, and the assumption that the spatial gradient of sediment transport drives morphological change, Yalin (1971, his Eq. (6.78)) derived the following time scale:

$$\frac{T_{nature}}{T_{lab}} = \frac{\sigma_h^2}{mI} \tag{29}$$

where σ_h = the length scale for depth, and m = distortion is typically larger than unity. Clearly this time scale is quite different from the time scale based on Froude scaling presented in the previous section.

Along similar lines, and by incorporation of distortion through the Strickler flow resistance relation, Tsujimoto (1990) derived a time scale that again differs from the above:

$$\frac{T_{nature}}{T_{lab}} = \sigma_L \sigma_h^{3/2} \sigma_D^{-7/6} = m\sigma_L^{5/2} \sigma_D^{-7/6} \tag{30}$$

where $\sigma_D^{-7/6}$ is the scale of bed particle size. This morphological time scale differs considerably from the Yalin time scale and the hydrodynamic time scale derived earlier ($\approx\sqrt{\sigma_L}$).

The time scales listed above refer to the vertical adaptation of the bed, and were designed for situations with fixed banks. In laterally mobile systems, the channel banks are not fixed, and bank erosion and formation affect the time scale of channel adjustment. For this paper the purpose remains to calculate a characteristic time scale of river bar and bend formation. We could propose to simply divide the volume of an entire meander bend by the channel sediment transport rate to derive a formative time scale. However, this simple approach is not applicable to the formation of bars and bends. The key problem is that braid bars and point bars are not formed as perfect sediment traps from the total transport rate but rather arise owing to two-dimensional gradients in transport rate. In other words, some residual transverse transport component determines the rate of morphological adaptation, and its characteristic time scale. The transverse transport rate is commonly an order of magnitude smaller than the total rate, and depends on helical flow and sediment mobility (Struiksma et al., 1985). To illustrate this it is insightful to compare the two in a hypothetical meander bend with an initially plane bed. This bed with level z will develop a slope dz/dn in transverse direction n, which means that at least a wedge-shaped volume of sediment is displaced of

$$V = \frac{W}{2}\frac{dz}{dn} \tag{31}$$

in m^2/m (per metre streamwise length). The near-bed shear stress vector is, in that case, directed slightly toward the inner bend because of helical flow driven by channel curvature, whilst the main flow direction is parallel to the curved channel. This small deviation between near-bed flow and main flow angles leads to a streamwise, and a transverse sediment transport component where it is immediately obvious that the streamwise transport rate is much larger than the transverse component. Yet it is the transverse component that will build up the transverse bed slope. For alternate bars, and for transverse bed slopes in bends with fixed banks, a characteristic time scale was derived by Crosato (2008) on the basis of Struiksma et al. (1985), here extended with intermittency:

$$T_{bar} = \frac{\lambda_s h}{I q_s} = \frac{\alpha_\theta}{\pi^2}\sqrt{\theta}\frac{W^2}{I q_s} \tag{32}$$

assuming resonant conditions with $\lambda_s = \lambda_w$. Assuming that the sediment mobility and therefore transport rate are the same but also that the direction of the sediment transport vector is the same despite distortion, this reduces approximately to

$$\frac{T_{nature}}{T_{lab}} \approx \frac{\sigma_W^2}{I} \tag{33}$$

which is similar to the Yalin time scale (Eq. (29)).

This time scale is insightful because it points to the important roles of the transverse bed slope effect on sediment transport and bar formation. This is directly applicable in experiments with pre-formed curved channels, where the morphological adaptation is limited to the transverse bed slope development. However, in the type of experiments that we are concerned with, bars and bends form, and migrate as part of the process, which means that the erodibility of the banks, and the rate of floodplain formation partly determine the migration rate.

3.3. 'Loose' time-scaling by bend migration rate

Migrating meander bends, in contrast to small bed perturbations and channel bars, do not merely depend on some component of sediment transport in the channel. Rather, the time scale to migrate meander bends depends strongly on the erodibility of the banks (e.g., Camporeale et al., 2005; Crosato, 2007; Parker et al., 2011; Eke et al., 2014). Once the bank is eroded, a new scroll bar can form: the 'bank-pull' hypothesis. We could also argue that the formation of scrollbars drives bank erosion, and therefore the rate of formation of floodplain determines the bank erosion rate: the 'bar-push' hypothesis. Systematic experiments provided evidence against the bar-push hypothesis and supported the bank-pull hypothesis (van de Lageweg et al., 2014), but given the fact that a subtle balance exists between bank erosion and floodplain formation it is likely that this varies between rivers, and perhaps even between bends (Eke et al., 2014).

Conceptually, erosion of cohesive banks proceeds in two stages: bank toe erosion and bank top failure. Bank toe erosion is a function of the flow pattern and sediment transport gradient along the bank toe (Simon et al., 2000), which may be affected by the presence of slump blocks (Parker et al., 2011), rooting, and geological constraints. Bank stability is a function of bank height, a host of geotechnical parameters of the bank soil, and the density of vegetation on the bank, and the density and depth of rooting in the bank (Pollen-Bankhead and Simon, 2008). Thus the problem of meander migration through bank erosion brings in complications that make it unpractical and perhaps unfeasible to do analytical calculations. It also remains unclear to what extent the geotechnical bank failure models are valid at the experimental scale. Indeed rule-based numerical modelling of meander migration with a consideration of the rates of vegetation development and decay showed that reduced bank erosion rates owing to vegetation establishment decrease the meander migration rate, and alter the shape of the meanders, but the results are highly sensitive to the parametrization of the bank strength, even with highly simplified vegetation establishment rules (Perucca et al., 2007). Also, experiments show that the time scales of vegetation development and the return period of floods that uproot the vegetation determines the degree to which vegetation reduces bank erosion and increases flow resistance (Perona et al., 2012). Indeed, recent flume experiments in an outdoor stream laboratory show a high resilience of seedlings to floods depending on age, species, and burial and scour patterns across the sandbar (Kui et al., 2014).

As an empirical alternative, W.M. Van Dijk et al. (2012) assessed the equivalent erosion time in the field by comparing the time to rework their experimental floodplain with floodplains in the field. The floodplain in their experiment was completely regenerated over 260 h. This represents the time required to form and migrate meanders over a space of one wavelength and one meander amplitude, and can therefore be used as an average meander migration rate M. This regeneration process takes between 100 years and millennia in nature depending on the size of the chosen river, here the Allier in France and the Rhine at the Dutch–German border (W.M. Van Dijk et al., 2012). This estimate implies a time scale $T_{nature}/T_{lab} \approx 10^4$. However, this inductive method requires a priori knowledge of the migration rate in nature. If we assume a universal range of migration rates normalised as M/W, i.e., fractions of channel width per unit of time, then we can define

$$\frac{T_{nature}}{T_{lab}} = \frac{M_{lab}}{M_{nature}}\frac{W_{nature}}{W_{lab}} \tag{34}$$

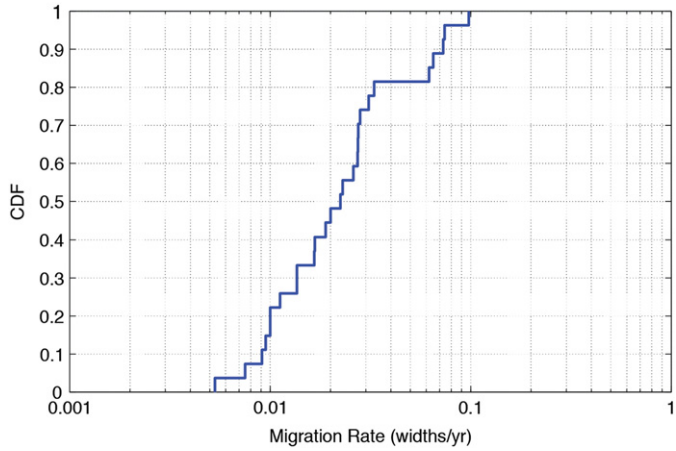

Fig. 7. Cumulative density function (CDF) of relative bend migration rates observed in 27 meandering gravel-bed rivers in nature, showing a spread of over an order of magnitude perhaps owing to various factors such as differences in bank strength relative to outer-bank bed shear stress.

which implicitly incorporates the intermittency I. A similar approach for alluvial fans with explicit incorporation of I is given in Cazanacli et al. (2002).

To test the value of a 'universal' range of migration rates, we show the cumulative distribution of channel migration rates for 27 gravel-bed meandering rivers in Fig. 7 (Braudrick, 2013). The migration rate data was collected from the literature including previous compilations where the channel width and grain size of the bed were known (e.g., Hickin and Nanson, 1984; MacDonald et al., 1991) as well as migration studies on individual rivers (e.g., Lewin, 1978; Micheli et al., 2004; Lauer and Parker, 2008), with most of the migration data obtained from comparing aerial photographs. The individual rivers and their morphology are given in Braudrick (2013), and the channels represent a large range in channel size and discharge. Their channel slopes (0.00019–0.012), bankfull discharge (7–5700), and bankfull widths (5–372 m) each range over nearly 3 orders of magnitude. The mean Shields stress (Eq. (2)) of the migrating rivers is 0.041, and the bed surface sediment diameter ranged from 4 to 75 mm. The time period, methods of measurement, and spatial extent of the measurements vary significantly, and some of the largest migration rates are measured for small rivers over one or two bends (e.g., the rivers in Allmendinger et al., 2005) and likely overstate migration rates of the longer reaches that make up the majority of the data set. The median migration rate from this data set is about 0.022 channel widths y^{-1} with a range from 0.005 to 0.1 widths y^{-1}. The duration of experiments and migration rates measured in experiments can now be used to estimate how many years the experiments represent (Table 3). Because migration rates and floodplain overturning rates can vary by over an order of magnitude, the corresponding time of experiments can vary widely as well but can at least provide an upper and lower bound on the corresponding duration in the field. Typical time scales of $T_{nature}/T_{lab} \approx 10^4 - 10^5$ arise, which are similar to the earlier estimate based on one sweep over the meander belt, and to the bar time scale T_{bar} in Table 2. Consequently, laboratory experiments of about 100 hour duration represent centuries to millennia in nature.

However, these time scales are again much different from those derived by various authors from similarity scaling (Table 2). This lack of consensus illustrates a lack of understanding, but also points at a confluence of several processes involved in channel migration (flow patterns, bank failure, bar building) that scale from the field to the

Table 2
Approximate scaling relations between the river Allier (France) (Kleinhans and van den Berg, 2011), and a typical experiment; see text for explanation of length adaptation scales, characteristic time scales, and flow resistance related to vegetation.

Variable	Symbol	Nature (Allier)	Scale	Experiment	Unit
Slope	S	0.0006		0.0055	m/m
Discharge	Q	200		0.001	m^3/s
Intermittency	I	0.05		1	
Width	W	100	333	0.3	m
Depth	h	1.45	132	0.011	m
Distortion	m			2.5	–
Aspect	W/h	69		27	–
Velocity	u	1.38	5	0.3	m/s
Median particle	D_{50}	0.005	10	0.0005	m
Max particle	D_{90}	0.015	12	0.0013	m
Bed roughness	k_s	0.15		0.0013	m
Observed bar length	L_p	600	200	3	m
Backwater adapt.	λ_{bw}	810	1209	0.67	m
Froude	Fr	0.37		0.91	–
Reynolds	Re	1700		3	10^3–
Grain Chezy	C'	55	1.5	36	$\sqrt{m}/s$
Grain Shields	θ'	0.08	1	0.08	–
Bed Chezy	C_b	37		36	$\sqrt{m}/s$
Total Shields	θ	0.17	2.1	0.08	–
Sediment transport	q_s	0.000068		0.000002	m^3/s
Bed defect celerity	c_b	2		7	m/day, m/h
Obs. meand. timesc. (Eq. (34))	T_{meand}	5000	1200	100	days, hrs
Froude-based timesc. (Eq. (25))	T_{Fr}		230		
Backw. timesc. (Eq. (27))	T_{bw}	410	102,500	0.096	days, h
Yalin timesc. (Eq. (29))	T_{bed}		92		
Tsujimoto timesc. (Eq. (30))	T_{bed}		688,000		
Struiksma timesc. (Eq. (32))	$T_{transverse}$	990	97,000	0.244	days, hrs
Stem density	m	10	0.0002	50,000	m^{-2}
Norm. stem density	see text	600	13	45	$10^3\ W^{-1}\ L_p^{-1}$
Stem diameter	D_t	0.025	50	0.0005	m
Vegetation density	d_v	0.25		25	m^{-1}
Drag coefficient	C_D	1		1	–
Trees	C_t	7.4		8.4	$\sqrt{m}/s$
Total	C_{tot}	7.3		8.2	$\sqrt{m}/s$

laboratory at different rates, thereby providing a range of scaling parameters. For individual experiments, determining the physical or biological processes that limit the migration rate (e.g., bank-pull versus bar-push) might point toward the most useful time-scaling approach.

Summarising, scaling time of experimental bars and meanders is quite uncertain, not merely because the scaling relations have not been fully worked out but also because the interactions in nature of processes of bank erosion, floodplain formation, and bar formation in the channel are not well understood yet. This requires further study, which can at least partly be done on the basis of available experimental data, models and field studies.

4. Scaling of riparian vegetation

4.1. Settling, growth, and mortality

The effects of vegetation on morphodynamics are manifold, and interactions are complicated by various feedbacks on vegetation settling, growth, and mortality (e.g., Gurnell et al., 2012). In particular, vegetation causes flow resistance and may enhance near-bed turbulence (e.g., Baptist et al., 2006) and rooting adds strength to river bars and floodplains (Pollen-Bankhead and Simon, 2008). Much of the morphological and engineering literature on the interactions between morphodynamics and vegetation are limited to situations where vegetation is assumed present in a static form that causes flow resistance. This was a prudent approach because the settling, survival, growth, and mortality of vegetation were insufficiently understood for the purpose of quantitative spatial modelling. Recent efforts target these unknowns in field measurements and field experiments (Kui et al., 2014; Pasquale et al., 2014), and in numerical modelling with explicit description of the life cycle of riparian eco-engineering tree species (van Oorschot et al., 2014). Here, eco-engineering species significantly change their environment, for example by increasing flow resistance, capture, stabilisation, or mobilisation of sediment and by increasing the stability of channel banks. Experiments including live plants are generally simplistic despite the fact that experiments employ real rather than virtual materials, and can therefore use live plants. In many cases a single species, often alfalfa, was seeded uniformly under low-flow conditions onto an evolving fluvial landscape, and allowed to sprout before a high flow was turned back on (Gran and Paola, 2001; Braudrick et al., 2009; Tal and Paola, 2010). This ignores the natural selection and settlement of vegetation by flow, and other dispersal mechanisms on suitable locations, and multiple species with different eco-engineering properties and ignores the selection from many seedlings to a smaller number of fully grown trees under competition between species, and under competition for water, light, and nutrients (for review, see Gurnell et al., 2012).

Yet the simplest possible protocol of uniform seeding and undisturbed development of a single species during low flow, which had to be done first in order to have experimental control, already gives remarkably complex and insightful results (Gran and Paola, 2001; Braudrick et al., 2009; Tal and Paola, 2010) (also compare Figs. 2 and 3). The expected finding was that the presence of vegetation reduces lateral migration of experimental rivers by adding bank strength, and focusing flow off the floodplain into the channel. However, a rather unexpected finding was that this caused avulsive behaviour and sediment pulsing. Channels with vegetated banks cannot readily adapt to changing upstream discharge and sediment feed, so that such changes cause in-channel sedimentation that leads to avulsion despite the presence of vegetation on the floodplains (Tal and Paola, 2010). More complex experiments added further surprises. For instance, W. van Dijk et al. (2013) found a remarkably different morphological response to two different modes of seed distribution: uniformly seeded alfalfa enhanced the tendency to meander, whereas alfalfa seeds distributed by the flowing water during floods caused the formation of many stable threads with islands protected by vegetation.

Furthermore, laboratory conditions, not entirely controlled in the recent experiments, appear to affect the survival or mortality of alfalfa. In W. van Dijk et al. (2013) the vegetation died rather quickly; it survived longer in Tal and Paola (2010); and in Braudrick et al. (2009) it continued to develop branched root systems that strengthened the bed even further. Indeed, experiments with force measurement at uprooting by Edmaier et al. (2014) showed a strong dependence of the necessary work on the development of the species-dependent secondary root system, in addition to moisture content and sediment size. These differences are all because of different lighting and moisture conditions (Van de Lageweg et al., 2010; Clarke, 2014), but we cannot exclude differences between batches of seeds, and fungi in the soil (Kleinhans et al., 2014).

Even in a simple experiment with uniformly seeded alfalfa sprouts, the vegetation growth adds biological dynamics with a specific time scale to the system, $T_{develop}$. This characterises the sprouting from seeds to fully grown sprouts (with at most two or four leaves) that survive a flood or other disturbance that occurs at typical recurrence interval $T_{disturbance}$ (Perucca et al., 2007; Tal and Paola, 2007; Perona et al., 2012). Defining a dimensionless time scale for potential survival of vegetation is therefore convenient:

$$\tau* = \frac{T_{develop}}{T_{disturbance}} \tag{35}$$

where $\tau* < 1$ means that vegetation likely does not survive the disturbance, and $\tau* > 1$ means likely survival. Most experiments to date were designed for survival to study effects of vegetation on river planform pattern and dynamics.

To summarise, different seed distribution strategies simulate different types of eco-engineers, but many habitats remain uncovered by the species most often used to date. The considerable effect of the seed distribution method opens up possibilities to experiment with seed releases during river flood pulses to stimulate plant settlement in specific habitats in the experiments. This would also require scaling of the flood pulses with the force needed to uproot a specific plant species of a certain age class. Furthermore, these experiments would benefit from a multiple number of species that are sensitive to the small water depth differences in the experiments to simulate different eco-engineers in contrasting habitats. Also, it remains to be studied what part of the plant population in meandering and braided rivers is uprooted by flow during floods (Edmaier et al., 2014) or uprooted because of bank migration (W. van Dijk et al., 2013), in the laboratory and in the field.

Table 3
Approximate scaling of experimental time by bend migration; based on the range of observed lateral migration rates M/W in the field, the experimental rate, and experiment duration, a minimum, and maximum time scale, and representative time in nature are calculated for three experiments; the Ganga river, although a sand-bed river, is included to extend the range of scales (Gupta et al., 2014).

Nature	M/W	M/W	Q
Unit	Min yr^{-1}	Max yr^{-1}	m^3/s
Allier	0.05	0.3	500
Rhine	0.005	0.02	2500
Ganga	0.1	0.27	45,000
rivers	0.005	0.1	

Laboratory	M/W	Duration	T_{nature}/T_{lab}	T_{nature}/T_{lab}	Time	Time
Unit	h^{-1}	h	Max–	Min–	Max yr	Min yr
Braudrick	0.048	136	84,000	4200	1300	70
vDijk1	0.5	260	876,000	43,800	26,000	1300
vDijk2	0.04	120	70,000	3500	1000	50

4.2. Hydraulic resistance from vegetation

Direct geometrical comparison of riparian plants and trees with alfalfa suggests that alfalfa represents considerable sized trees (Table 2). For a scale of $\sigma_W = 200/0.20 = 1000$, a 0.5 mm stem thickness translates to a tree stem diameter of 0.5 m, which would only occur in relatively mature riparian forests as found on the outside of meander bends or on the older parts of point bars. However, the eco-engineering effect of the species rather than the size matters and the mismatch between the scales. Perhaps the flow resistance induced by a single seedling in an experiment represents the flow resistance effect of a large patch of vegetation in nature, particularly for flow over point bars, where the vegetation tends to be younger and hence smaller.

The effective flow resistance of riparian trees in a natural river such as the Allier, and alfalfa in experiments can be compared directly with the vegetation resistance relation of Baptist et al. (2006) for emergent trees:

$$C_t = \sqrt{\frac{2g}{C_D m D_t h}} \tag{36}$$

so that the total flow resistance including the bare bed surface friction (Eq. (4)) becomes

$$C_{tot} = \sqrt{\frac{1}{C_b^{-2} + C_t^{-2}}}. \tag{37}$$

The chosen parameters listed in Table 2 are based on casual observations of vegetation in the river Allier and typical experimental conditions. The drag coefficient is taken at unity but in reality depends on plant geometry, number and type of leaves, and flow conditions (Aberle and Järvelä, 2013).

The striking result of this simple calculation is that the different variables may compensate the differences between nature and the experiments. Per square metre, the sparse vegetation in the river Allier results in the same Chezy flow resistance as in the experiments when that has a relatively large seeding density. However, to better understand how this scales with river dimensions the number of plants is also normalised by bar area, calculated conservatively as observed bar length times channel width, as a representative surface area. This reverses the proportions between experiment and river: the natural river requires a much larger number of tree stems *per bar* than the experimental river to attain the same hydraulic resistance. This can be seen as that a single alfalfa sprout in an experiment causes the same flow resistance as a group of small riparian trees in nature. This implies a scaling effect: apparently the effect of vegetation on hydraulic resistance is exaggerated in experiments with alfalfa when the vegetation density is directly compared between experiments and field situations.

4.3. Bank strength from vegetation

Added strength from rooting has been studied in detail for full-scale conditions (e.g., Pollen-Bankhead and Simon, 2008). For experiments, root structure, and plant density may be different as the plants are geometrically oversized. However, a more important variable is the rooting depth on the banks relative to the channel depth, which determines the possibility for undercutting (Pollen-Bankhead and Simon, 2008; Perona et al., 2012):

$$\lambda_* = \frac{L_{rootingdepth}}{L_{bankheight}} \tag{38}$$

where $\lambda_* > 1$ means that vegetation likely prevents undercutting of banks so that the channel is laterally fixed, whereas $\lambda_* < 1$ means that banks can be undercut so that bank retreat by failure of vegetated banks is possible.

No models are currently available to predict bank erosion rates and the concurrent time scale of meander migration with vegetated floodplain. However, two experimental setups have been developed recently that can be used for dedicated experimental determination of bank strength depending on flow conditions, sediment characteristics, and vegetation characteristics. The first one is the 'Friedkin' setup, where flow is directed at an angle of 45° onto a block of sediment (Friedkin, 1945). This setup was extensively tested and successfully applied to vegetated banks in Kleinhans et al. (2014). However, a disadvantage is that bend flow is not fully developed, and a boundary layer forms at the bank because of the sudden transition from clear water flow in a rough channel to the erosive channel bank. Furthermore, the bank is always undercut by clear water scour because no sediment was supplied upstream.

The second setup we developed is an annular flume with a channel on a circular floodplain (Fig. 8, developed by RT and MGK). The advantage of this setup is that, despite its small size, conditions along the channel of constant curvature are uninterrupted by an upstream and downstream boundary. This also means that the bed sediment transport is in equilibrium, and bank undercutting proceeds entirely because of the three-dimensionality of the flow in the channel. As such, the setup is complementary to the Friedkin experiment. The flow in the channel is driven by paddles touching the water surface, and the water level in the flume determines the floodplain inundation level. The inevitable result of driving the flow by surface paddles or drag is that a helical flow sets up, which initiates inner-bend bar formation (for review, see Sumner et al., 2008). The floodplain was made of hard clay for flow testing only and of cohesionless sand for bank erosion tests. Alfalfa was seeded uniformly onto the sandy floodplain at known densities to test bank erosion rates and to study flow and bank erosion processes qualitatively.

Two surprising results emerged from the annular flume study. The first is that a complex floodplain flow pattern of circulating cells emerged (Fig. 9). If such patterns form in larger-scale experiments, then this could transport floodplain fines at preferential paths onto the floodplain. The second surprising result was that not only rooting but also overhanging vegetation protected the banks against erosion. This was also observed in the Friedkin experiments (Kleinhans et al.,

Fig. 8. Setup of the annular flume with a floodplain. The diameter of the entire circular basin is 0.8 m. The radius of the channels is 0.2 m, and the initial width, and depth are 11.2, and 1.2 cm, respectively. The flow is driven by 12 paddles touching the water surface with velocities between 0.05 and 0.63 m/s, which means flow remained subcritical, and was transitional to turbulent.

2014) and by Braudrick et al. (2009). Some alfalfa sprouts hang downward over the bank, which increased near-bank flow resistance that reduced bank erosion. We were yet unable to isolate the effects of root reinforcement and flow resistance enhancement. Regardless of this, the banks in the Friedkin experiments eroded much faster (a few channel widths per hour) than in the annular flume (a small fraction of the channel width per hour) in comparable conditions, presumably because in the former sediment was not supplied toward the bank, and in the latter there was. Unsurprising results are that the channel banks are generally much stronger than cohesionless sand with vegetation and are already unerodible at a seeding density of 3 cm^{-2} (Fig. 10). This experimental setup has potential for a detailed study of effects of vegetation on flow and bank erosion processes in an annular channel.

To summarise, the elementary scaling considerations and experimental results in this chapter clearly indicate that a host of relevant questions needs to be, and can be, addressed in future experiments. This includes the effects of multiple vegetation species with different habitats, seeding for a range of τ_* and λ_*, settling patterns in relation to morphological patterns in the self-formed floodplain, and effects of resilience against disturbances such as uprooting by strong flows, inundation duration and burial. Such experiments will require us to control the rates of growth and mortality in the sprouting phase, which have their own time scales.

5. Conclusions

We tested whether braiding index and length scales of bars and bends depend on the size of the river, and we reviewed methods to estimate the time scale of bar and bend migration. Both depend critically on floodplain strength.

From a combination of a linear bar theory with hydraulic geometry relations valid for the entire range of small experiments to large rivers, we found no scale effects in the sense that bar length relative to channel width changes as a function of scale when width–depth ratio and sediment mobility are the same as in nature. This means that the geometric proportions of experimental rivers with bars and bends are effectively the same as those in nature, given relatively the same bank strength. This result is somewhat sensitive to the hydraulic geometry relations that bulk the effects of hydraulic resistance and bank strength relations into empirical parameters. This shows that scale effects in experiments are likely to come from floodplain processes rather than in-channel processes.

Time-scaling approaches in classical similarity scaling methods are derived from sediment transport gradients over a certain control volume. However, time scales reported in literature for vertical bed elevation change, although derived from theory, differ in orders of magnitude, reflecting a lack of understanding. Moreover, bar and bend migration are governed by lateral bank retreat rates rather than vertical bed-level change. Bank retreat depends on a range of geotechnical processes other than sediment transport owing to cohesive floodplain sediment and riparian vegetation. This makes bank retreat vary an order of magnitude between different rivers, and between similarity methods, and measurements in experiments, which is not well predictable from channel process scaling. Pending further progress, experimental bank retreat rate can well be measured in dedicated auxiliary experiments.

A review of the properties of vegetation used in experiments and a novel auxiliary experiment showed that flow resistance, bank stability,

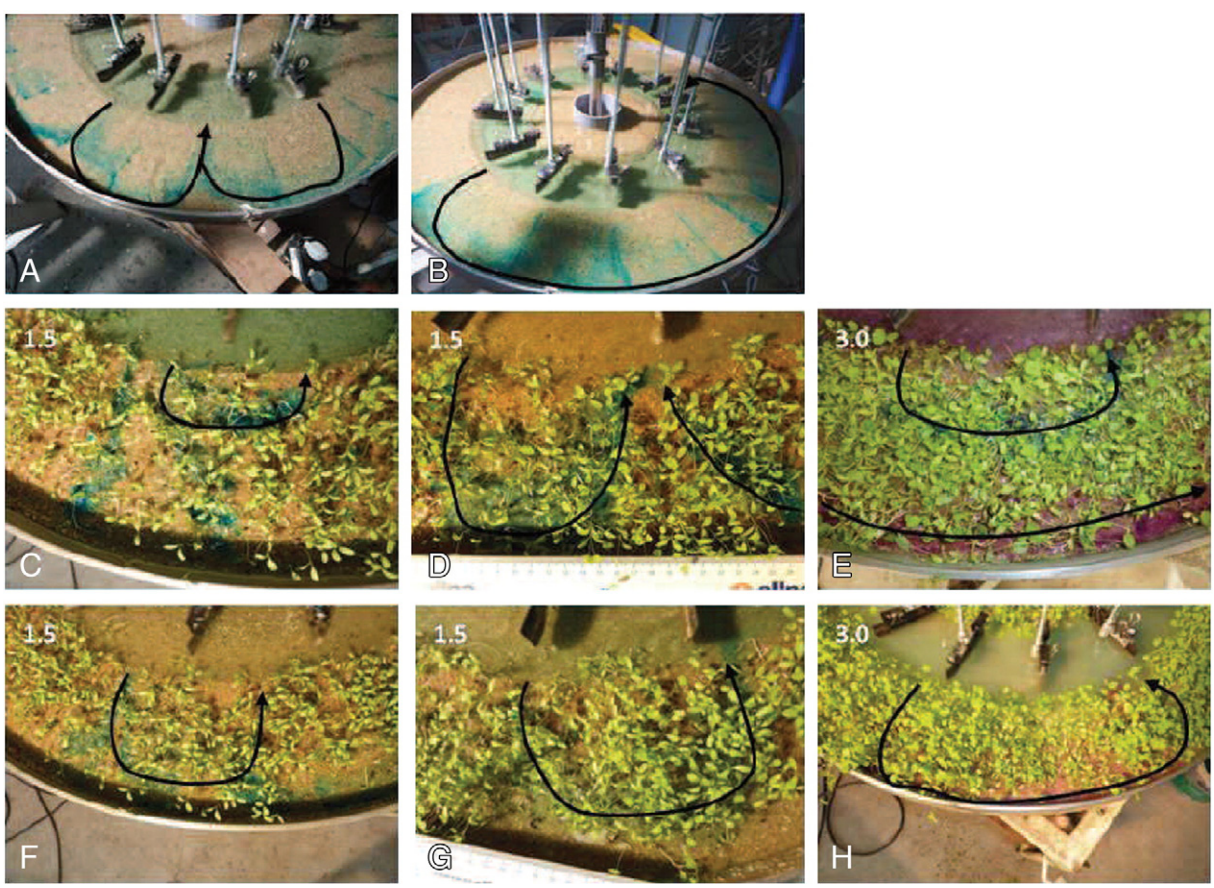

Fig. 9. Flow patterns on the floodplain for different vegetation densities, and inundation depths. Floodplain flow was laminar in all cases. (A) 2 mm floodplain inundation, sand only. (B) 4 mm floodplain inundation, sand only. (C) 2 mm floodplain inundation, 6 day old alfalfa seeded at 1.5 cm^{-2}. (D) 2 mm floodplain inundation, 15 day old alfalfa seeded at 1.5 cm^{-2}. (E) 2 mm floodplain inundation, 15 day old alfalfa seeded at 3 cm^{-2}. (F) 4 mm floodplain inundation, 6 day old alfalfa seeded at 1.5 cm^{-2}. (G) 4 mm floodplain inundation, 15 day old alfalfa seeded at 1.5 cm^{-2}. (H) 4 mm floodplain inundation, 15 day old alfalfa seeded at 3 cm^{-2}.

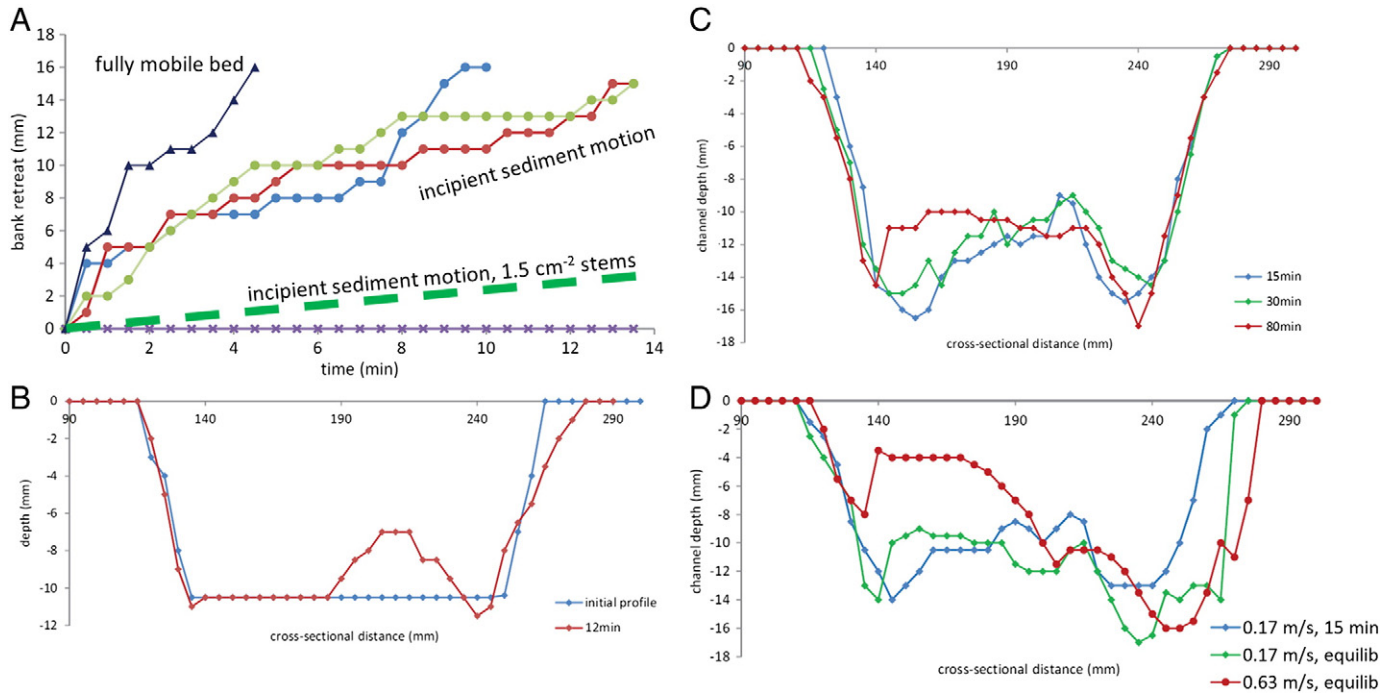

Fig. 10. Bank erosion in the annular flume. (A) Bank retreat over time for bare, and vegetated banks (seeding density 3 cm^{-2}). (B) Cross-sectional profile with unvegetated floodplain at incipient motion (water surface flow velocity 0.17 m/s). (C) Cross-sectional profiles for densely vegetated floodplain (3 cm^{-2}) at fully mobile bed (water surface flow velocity 0.63 m/s). (D) Same as (C) for low vegetation density (1.5 cm^{-2}).

and retreat rate can be well constrained for given vegetation sprout density on the floodplain. However, natural vegetation dynamics, such as spatial and temporal distributions of different species in different flow conditions and substrates as found in nature, are relatively simplistically represented in experiments. Here the most important scale parameters are the length of the roots compared to channel depth and the characteristic time scale for growth of vegetation relative to the recurrence interval of floods. Perhaps more spatial variation in settlement and growth stages can be attained by a more realistic protocol of flood magnitude and duration and with seeding at particular flow stages or by supplying seeds to the upstream boundary rather than seeding manually. Furthermore, a search for other plant species is needed that are more sensitive to variations in conditions and substrate at the scale of laboratory experiments.

Finally, this paper showed that the *materiality* of 'Lilliputian' river systems created in laboratory experiments, as opposed to *virtuality* of numerical models, is a guarantee for surprising and interesting results that raise new questions about, and enhance our understanding of, the biomorphodynamics of the 'Giant' fluvial systems in nature.

Acknowledgements

We gratefully acknowledge two anonymous reviewers and the associate editor for constructive comments that helped to improve the paper. Nico Struiksma is cordially acknowledged for discussion about a morphological time scale of meander bends. MGK and WMvD were supported by the Netherlands Organisation for Scientific Research (NWO) (grant ALW-VIDI-864.08.007 to MGK). WIvdL was supported by Exxon Mobil Upstream Research (grant EM01734 to MGK and George Postma). MvO contributed to the discussion of experimental vegetation, and was supported by the EU-FP7 REFORM project (grant to Tom Buijse of Deltares). RT did the annular flume experiments with MGK as part of his B.Sc. thesis.

References

Aberle, J., Järvelä, J., 2013. Flow resistance of emergent rigid and flexible floodplain vegetation. J. Hydraul. Res. 51, 33–45. http://dx.doi.org/10.1080/00221686.2012.754795.

Allmendinger, N.E., Pizzuto, J.E., Potter, N., Johnson, T.E., Hession, W.C., 2005. The influence of riparian vegetation on stream width, eastern Pennsylvania, USA. Geol. Soc. Am. Bull. 117, 229–243. http://dx.doi.org/10.1130/B25447.1 (URL: http://gsabulletin.gsapubs.org/content/117/1-2/229.abstract).

Ashmore, P., 1982. Laboratory modelling of gravel braided stream morphology. Earth Surf. Process. Landf. 7, 201–225.

Baptist, M., Babobic, V., Rodriguez Uthurburu, J., Keijzer, M., Uittenbogaard, R., Mynett, A., Verwey, A., 2006. On inducing equations for vegetation resistance. J. Hydraul. Res. 45, 1–16.

Bertoldi, W., Zanoni, L., Tubino, M., 2009. Planform dynamics of braided streams. Earth Surf. Process. Landf. 34, 547–557. http://dx.doi.org/10.1002/esp.1755.

Braudrick, C., 2013. Experimental Meandering in Coarse-bedded Rivers. Ph.D. thesis.

Braudrick, C., Dietrich, W., Leverich, G., Sklar, L., 2009. Experimental evidence for the conditions necessary to sustain meandering in coarse-bedded rivers. PNAS 106, 936–941.

Camporeale, C., Perona, P., Porporato, A., Ridolfi, L., 2005. On the long-term behavior of meandering rivers. Water Resour. Res. 41, W12403. http://dx.doi.org/10.1029/2005WR004109.

Cazanacli, D., Paola, C., Parker, G., 2002. Experimental steep, braided flow: application to flooding risk on fans. J. Hydraul. Eng. 128, 322–330.

Clarke, L.E., 2014. The use of live vegetation in geomorphological experiments: how to create optimal growing conditions. Earth Surf. Process. Landf. 39, 705–710. http://dx.doi.org/10.1002/esp.3534.

Crosato, A., 2007. Effects of smoothing and regridding in numerical meander migration models. Water Resour. Res. 43, W01401. http://dx.doi.org/10.1029/2006WR005087.

Crosato, A., 2008. Analysis and Modelling of River Meandering. Published PhD thesis, Delft University of Technology. IOS Press, Amsterdam.

Crosato, A., Mosselman, E., 2009. Simple physics-based predictor for the number of river bars and the transition between meandering and braiding. Water Resour. Res. 45, W03424. http://dx.doi.org/10.1029/2008WR007242.

de Villiers, G., Kleinhans, M.G., Postma, G., 2013. Experimental delta formation in crater lakes and implications for interpretation of Martian deltas. J. Geophys. Res. 118, 651–670. http://dx.doi.org/10.1002/jgre.20069.

de Vries, M., Klaassen, G., Struiksma, N., 1990. On the use of movable bed models for river problems: a state-of-the-art. Int. J. Sediment Res. 5, 35–47.

Eaton, B., Church, M., 2007. Predicting downstream hydraulic geometry: a test of rational regime theory. J. Geophys. Res. 112, F03025. http://dx.doi.org/10.1029/2006JF000734.

Eaton, B., Giles, T., 2009. Assessing the effect of vegetation-related bank strength on channel morphology and stability in gravel-bed streams using numerical models. Earth Surf. Process. Landf. 34, 712–724. http://dx.doi.org/10.1002/esp.1768.

Edmaier, K., Crouzy, B., Ennos, R., Burlando, P., Perona, P., 2014. Influence of root characteristics and soil variables on the uprooting mechanics of *Avena sativa* and *Medicago sativa* seedlings. Earth Surf. Process. Landf. 39, 1354–1364. http://dx.doi.org/10.1002/esp.3587.

Egozi, R., Ashmore, P., 2008. Defining and measuring braiding intensity. Earth Surf. Process. Landf. 33, 2121–2138. http://dx.doi.org/10.1002/esp.1658.

Egozi, R., Ashmore, P., 2009. Experimental analysis of braided channel pattern response to increased discharge. J. Geophys. Res. 114, F02012. http://dx.doi.org/10.1029/2008JF001099.

Eke, E., Parker, G., Shimizu, Y., 2014. Numerical modeling of erosional and depositional bank processes in migrating river bends with self-formed width: morphodynamics of bar push and bank pull. J. Geophys. Res. Earth Surf. 119, 1455–1483. http://dx.doi.org/10.1002/2013JF003020.

Ferguson, R., 1987. Hydraulic and sedimentary controls of channel pattern. In: Richards, K. (Ed.), River Channels: Environment and Process. Blackwell, Oxford, UK, pp. 129–158.

Friedkin, J., 1945. A Laboratory Study of the Meandering of Alluvial Rivers. U.S. Army Corps of Engineers, U.S. Waterways Experiment Station, Vicksburg, Mississippi, USA.

Fujita, Y., 1989. Bar and channel formation in braided streams. In: Ikeda, S., Parker, G. (Eds.), River Meandering. American Geophysical Union, Washington D.C., pp. 417–462.

Gardner, J., Ashmore, P., 2011. Geometry and grain-size characteristics of the basal surface of a braided river deposit. Geology 39, 247–250. http://dx.doi.org/10.1130/G31639.1.

Geerling, G., Ragas, A., Leuven, R., van den Berg, J., Breedveld, M., Liefhebber, D., Smits, A., 2006. Succession and rejuvenation in floodplains along the river Allier (France). Hydrobiologia 565, 71–86.

Gran, K., Paola, C., 2001. Riparian vegetation controls on braided stream dynamics. Water Resour. Res. 37, 3275–3283.

Grant, G., 1997. Critical flow contrains flow hydraulics in mobile-bed streams: a new hypothesis. Water Resour. Res. 33, 349–358.

Gupta, N., Kleinhans, M., Addink, E., Atkinson, P., Carling, P., 2014. One-dimensional modeling of a recent Ganga avulsion: assessing the potential effect of tectonic subsidence on a large river. Geomorphology 213, 24–37. http://dx.doi.org/10.1016/j.geomorph.2013.12.038.

Gurnell, A., Bertoldi, W., Corenblit, D., 2012. Changing river channels: the roles of hydrological processes, plants and pioneer fluvial landforms in humid temperate, mixed load, gravel bed rivers. Earth Sci. Rev. 111, 129–141. http://dx.doi.org/10.1016/j.earscirev.2011.11.005.

Hickin, E., Nanson, G., 1984. Lateral migration rates of river bends. J. Hydraul. Eng. 110, 1557–1567. http://dx.doi.org/10.1061/(ASCE)0733-9429(1984)110:11(1557).

Hoyal, D., Sheets, B., 2009. Morphodynamic evolution of experimental cohesive deltas. J. Geophys. Res. 114, F02009. http://dx.doi.org/10.1029/2007JF000882.

Hughes, S., 1993. Physical models and laboratory techniques in coastal engineering. Advanced Series on Ocean Engineering. World Scientific vol. 7.

Hundey, E.J., Ashmore, P.E., 2009. Length scale of braided river morphology. Water Resour. Res. 45, W08409. http://dx.doi.org/10.1029/2008WR007521.

Ikeda, S., 1982. Lateral bed load transport on side slopes. J. Hydraul. Div. ASCE 108, 1369–1373.

Kleinhans, M.G., 2010. Sorting out river channel patterns. Prog. Phys. Geogr. 34, 287–326. http://dx.doi.org/10.1177/0309133310365300.

Kleinhans, M.G., van den Berg, J.H., 2011. River channel and bar patterns explained and predicted by an empirical and a physics-based method. Earth Surf. Process. Landf. 36, 721–738. http://dx.doi.org/10.1002/esp.2090.

Kleinhans, M.G., Buskes, C., de Regt, H., 2005. Terra incognita: explanation and reduction in earth science. Int. Stud. Philos. Sci. 19, 289–317. http://dx.doi.org/10.1080/02698590500462356.

Kleinhans, M.G., van Dijk, W., van de Lageweg, W., Hoyal, D., Markies, H., van Maarseveen, M., Roosendaal, C., van Weesep, W., van Breemen, D., Hoendervoogt, R., Cheshier, N., 2014. Quantifiable effectiveness of experimental scaling of river- and delta morphodynamics and stratigraphy. Earth Sci. Rev. 133, 43–61. http://dx.doi.org/10.1016/j.earscirev.2014.03.001.

Kui, L., Stella, J., Lightbody, A., Wilcox, A., 2014. Ecogeomorphic feedbacks and flood loss of riparian tree seedlings in meandering channel experiments. Water Resour. Res. 50, 9366–9384. http://dx.doi.org/10.1002/2014WR015719.

Lauer, J., Parker, G., 2008. Net local removal of floodplain sediment by river meander migration. Geomorphology 96, 123–149. http://dx.doi.org/10.1016/j.geomorph.2007.08.003.

Leddy, J., Ashworth, P., Best, J., 1993. Mechanisms of Anabranch Avulsion Within Gravel-bed Braided Rivers: Observations From a Scaled Physical Model Special Publication No. 75. pp. 119–127.

Leopold, L., Wolman, M., 1957. River Channel Patterns: Braided, Meandering and Straight 282-B.

Lewin, J., 1978. Meander development and floodplain sedimentation: a case study from mid-wales. Geol. J. 13, 25–36. http://dx.doi.org/10.1002/gj.3350130104.

MacDonald, T., Parker, G., Luethe, D., 1991. Inventory and analysis of stream meander problems in Minnesota. Technical Report. St. Anthony Falls Hydraulic Laboratory (Retrieved from the University of Minnesota Digital Conservancy, http://purl.umn.edu/108225).

Malverti, L., Lajeunesse, E., Métivier, F., 2008. Small is beautiful: upscaling from microscale laminar to natural turbulent rivers. J. Geophys. Res. 113, F04004. http://dx.doi.org/10.1029/2007JF000974.

Maynord, S., 2006. Evaluation of the micromodel: an extremely small-scale movable bed model. J. Hydraul. Eng. 132, 343–353. http://dx.doi.org/10.1061/(ASCE)0733-9429(2006)132:4(343).

Meyer-Peter, E., Mueller, R., 1948. Formulas for bed-load transport. Proceedings 2nd Meeting, Int. Ass. for Hydraulic Structures Res., Stockholm, Sweden, pp. 39–64.

Micheli, E.R., Kirchner, J.W., Larsen, E.W., 2004. Quantifying the effect of riparian forest versus agricultural vegetation on river meander migration rates, central Sacramento river, California, USA. River Res. Appl. 20, 537–548. http://dx.doi.org/10.1002/rra.756.

Morgan, M., 2003. Experiments without material intervention: model experiments, virtual experiments, and virtually experiments. In: Radder, H. (Ed.), The Philosophy of Scientific Experimentation. University of Pittsburgh Press, Pittsburgh, USA, pp. 216–235 (chapter 11).

Oreskes, N., Shrader-Frechette, K., Belitz, K., 1994. Verification, validation and confirmation of numerical models in the earth sciences. Science 263, 641–642.

Paola, C., Straub, K., Mohrig, D., Reinhardt, L., 2009. The "unreasonable effectiveness" of stratigraphic and geomorphic experiments. Earth Sci. Rev. 97, 1–43. http://dx.doi.org/10.1016/j.earscirev.2009.05.003.

Parker, G., 2004. 1D sediment transport morphodynamics with applications to rivers and turbidity currents. URL: http://www.cee.uiuc.edu/people/parkerg/morphodynamics_e-book.htm.

Parker, G., Paola, C., Whipple, K., Mohrig, D., 1998. Alluvial fans formed by channelized fluvial and sheet flow. I: theory. J. Hydraul. Eng. 124, 985–995.

Parker, G., Wilcock, P., Paola, C., Dietrich, W.E., Pitlick, J., 2007. Physical basis for quasi-universal relations describing bankfull hydraulic geometry of single-thread gravel bed rivers. J. Geophys. Res. 112, F04005. http://dx.doi.org/10.1029/2006JF000549.

Parker, G., Shimizu, Y., Wilkerson, G.V., Eke, E.C., Abad, J.D., Lauer, J.W., Paola, C., Dietrich, W.E., Voller, V.R., 2011. A new framework for modeling the migration of meandering rivers. Earth Surf. Process. Landf. 36, 70–86. http://dx.doi.org/10.1002/esp.2113.

Pasquale, N., Perona, P., Francis, R., Burlando, P., 2014. Above-ground and below-ground Salix dynamics in response to river processes. Hydrol. Process. 28, 5189–5203. http://dx.doi.org/10.1002/hyp.9993.

Peakall, J., Ashworth, P., Best, J., 1996. Physical modelling in fluvial geomorphology: principles, applications and unresolved issues. In: Rhoads, B., Thorn, C. (Eds.), The Scientific Nature of Geomorphology. Wiley, Chichester, UK, pp. 221–253.

Peakall, J., Ashworth, P., Best, J., 2007. Meander-bend evolution, alluvial architecture, and the role of cohesion in sinuous river channels: a flume study. J. Sediment. Res. 77, 197–212. http://dx.doi.org/10.2110/jsr.2007.017.

Perona, P., Molnar, P., Crouzy, B., Perucca, E., Jiang, Z., McLelland, S., Wüthrich, D., Edmaier, K., Francis, R., Camporeale, C., Gurnell, A., 2012. Biomass selection by floods and related timescales: part 1. Experimental observations. Adv. Water Resour. 39, 85–96.

Perucca, E., Camporeale, C., Ridolfi, L., 2007. Significance of the riparian vegetation dynamics on meandering river morphodynamics. Water Resour. Res. 43, W03430. http://dx.doi.org/10.1029/2006WR005234.

Pollen-Bankhead, N., Simon, A., 2008. Enhanced application of root-reinforcement algorithms for bank-stability modeling. Earth Surf. Process. Landf. 33. http://dx.doi.org/10.1002/esp.1690.

Pyrce, R., Ashmore, P., 2005. Bedload path length and point bar development in gravel-bed river models. Sedimentology 52, 839–857. http://dx.doi.org/10.1111/j.1365-3091.2005.00714.x.

Reynolds, O., 1887. On Certain Laws Relating to the Regime of Rivers and Estuaries and on the Possibility of Experiments on a Small Scale. Br. Assoc. Rep., London, pp. 555–562.

Ribberink, J., Van der Sande, J., 1985. Aggradation in rivers due to overloading — analytical approaches. J. Hydraul. Res. 23, 273–283. http://dx.doi.org/10.1080/00221688509499355.

Schumm, S., Khan, H., 1972. Experimental study of channel patterns. Geol. Soc. Am. Bull. 83, 1755–1770.

Schumm, S., Mosley, M., Weaver, W., 1987. Experimental Fluvial Geomorphology. Wiley, New York, USA (413 pp.).

Schuurman, F., 2015. Bar and channel evolution within meandering and braiding rivers using physics-based modeling. Netherlands Geographical Studies. Utrecht University, Graduate School of Geosciences, Utrecht (URL: N/A).

Schuurman, F., Marra, W., Kleinhans, M.G., 2013. Physics-based modeling of large braided sand-bed rivers: bar pattern formation, dynamics and sensitivity. J. Geophys. Res. 118, 2509–2527. http://dx.doi.org/10.1002/2013JF002896.

Seminara, G., 2005. Meanders. J. Fluid Mech. 554, 271–297.

Sheets, B.A., Hickson, T.A., Paola, C., 2002. Assembling the stratigraphic record: depositional patterns and time-scales in an experimental alluvial basin. Basin Res. 14, 287–301.

Shvidchenko, A., Kopaliani, Z., 1998. Hydraulic modeling of bed load transport in gravel-bed Laba river. J. Hydraul. Eng. 124, 778–785.

Simon, A., Curini, A., Darby, S., Langendoen, E., 2000. Bank and near-bank processes in an incised channel. Geomorphology 35, 183–217.

Smith, C., 1998. Modeling high sinuosity meanders in a small flume. Geomorphology 25, 19–30.

Struiksma, N., 1986. Scale effects in the reproduction of the overall bed topography in river models. IAHR Symposium on Scale Effects in Modelling Sediment Transport Phenomena, Toronto, Canada.

Struiksma, N., Olesen, K., Flokstra, C., De Vriend, H., 1985. Bed deformation in curved alluvial channels. J. Hydraul. Res. 23, 57–79.

Sumner, J., Amy, L., Talling, P., 2008. Deposit structure and processes of sand deposition from decelerating sediment suspensions. J. Sediment. Res. 78, 529–547. http://dx.doi.org/10.2110/jsr.2008.062.

Tal, M., Paola, C., 2007. Dynamic single-thread channels maintained by the interaction of flow and vegetation. Geology 35, 347–350. http://dx.doi.org/10.1130/G23260A.1.

Tal, M., Paola, C., 2010. Effects of vegetation on channel morphodynamics: results and insights from laboratory experiments. Earth Surf. Process. Landf. 35, 1014–1028. http://dx.doi.org/10.1002/esp.1908.

Talmon, A., Struiksma, N., van Mierlo, M., 1995. Laboratory measurements of the direction of sediment transport on transverse alluvial-bed slopes. J. Hydraul. Res. 33, 495–517.

Tsujimoto, T., 1990. Distorted Model and Time Scale Evaluation of Multiscale Subjected Fluvial Processes. Kluwer Academic Publishers, The Netherlands, pp. 31–48.

Van de Lageweg, W.I., Van Dijk, W.M., Hoendervoogt, R., Kleinhans, M.G., 2010. Effects of riparian vegetation on experimental channel dynamics. In: Dittrich, Koll, Aberle, Geisenhainer (Eds.), Riverflow 2010 vol. 2. Bundesanstalt für Wasserbau, pp. 1331–1338.

van de Lageweg, W., van Dijk, W., Kleinhans, M., 2013. Channel belt architecture formed by an experimental meandering river. Sedimentology 60, 840–859. http://dx.doi.org/10.1111/j.1365-3091.2012.01365.x.

van de Lageweg, W., van Dijk, W., Baar, A., Rutten, J., Kleinhans, M., 2014. Bank pull or bar push: what drives scroll-bar formation in meandering rivers? Geology 42, 319–322. http://dx.doi.org/10.1130/G35192.1.

van Dijk, M., Kleinhans, M.G., Postma, G., Kraal, E., 2012a. Contrasting morphodynamics in alluvial fans and fan deltas: effect of the downstream boundary. Sedimentology 59, 2125–2145. http://dx.doi.org/10.1111/j.1365-3091.2012.01337.x.

Van Dijk, W.M., Van de Lageweg, W.I., Kleinhans, M.G., 2012b. Experimental meandering river with chute cutoffs. J. Geophys. Res. 117, F03023. http://dx.doi.org/10.1029/2011JF002314.

van Dijk, W., Teske, R., van de Lageweg, W., Kleinhans, M.G., 2013a. Effects of vegetation distribution on experimental river channel dynamics. Water Resour. Res. 49, 7558–7574. http://dx.doi.org/10.1002/2013WR013574.

Van Dijk, W.M., Van de Lageweg, W.I., Kleinhans, M.G., 2013b. Formation of a cohesive floodplain in a dynamic experimental meandering river. Earth Surf. Process. Landf. 38, 1550–1565. http://dx.doi.org/10.1002/esp.3400.

Van Dijk, W., Schuurman, F., Van de Lageweg, W., Kleinhans, M., 2014. Bifurcation instability and chute cutoff development in meandering gravel-bed rivers. Geomorphology 213, 277–291. http://dx.doi.org/10.1016/j.geomorph.2014.01.018.

van Oorschot, M., Kleinhans, M., Geerling, G., Middelkoop, H., Mosselman, E., Buijse, T., 2014. Distinct patterns of interactions between vegetation and river morphology. 10th Int. Symp. Ecohydraulics, Trondheim, Norway.

Wilcock, P., McArdell, B., 1997. Partial transport of a sand–gravel sediment. Water Resour. Res. 33, 235–245.

Yalin, M., 1971. Theory of Hydraulic Models. Macmillan, London, UK.